

UNIVERSITÉ DU QUÉBEC À MONTRÉAL

FLUX SÉDIMENTAIRES
LE LONG DE LA RIDE DE LOMONOSOV,
OCÉAN ARCTIQUE

MÉMOIRE
PRÉSENTÉ
COMME EXIGENCE PARTIELLE
DE LA MAÎTRISE EN SCIENCES DE LA TERRE

PAR
CYNTHIA LE DUC

DÉCEMBRE 2018

UNIVERSITÉ DU QUÉBEC À MONTRÉAL
Service des bibliothèques

Avertissement

La diffusion de ce mémoire se fait dans le respect des droits de son auteur, qui a signé le formulaire *Autorisation de reproduire et de diffuser un travail de recherche de cycles supérieurs* (SDU-522 – Rév.01-2006). Cette autorisation stipule que «conformément à l'article 11 du Règlement no 8 des études de cycles supérieurs, [l'auteur] concède à l'Université du Québec à Montréal une licence non exclusive d'utilisation et de publication de la totalité ou d'une partie importante de [son] travail de recherche pour des fins pédagogiques et non commerciales. Plus précisément, [l'auteur] autorise l'Université du Québec à Montréal à reproduire, diffuser, prêter, distribuer ou vendre des copies de [son] travail de recherche à des fins non commerciales sur quelque support que ce soit, y compris l'Internet. Cette licence et cette autorisation n'entraînent pas une renonciation de [la] part [de l'auteur] à [ses] droits moraux ni à [ses] droits de propriété intellectuelle. Sauf entente contraire, [l'auteur] conserve la liberté de diffuser et de commercialiser ou non ce travail dont [il] possède un exemplaire.»

REMERCIEMENTS

De nombreuses personnes ont contribué à la réalisation de cette recherche de maîtrise, que ce soit par leur travail, leur temps, leur appui ou leur encouragement. Je tiens tout d'abord à remercier ma directrice principale, Anne de Vernal, pour la confiance qu'elle m'a accordée dès le début de mon baccalauréat et qui m'a motivé à poursuivre des études supérieures, à me dépasser et réaliser mon plein potentiel. Je la remercie aussi pour les incroyables opportunités qu'elle m'a offertes tout au long de ma maîtrise qui m'ont permis de vivre des expériences exceptionnelles, de partager des moments inoubliables, de rencontrer des gens extraordinaires et d'enrichir mon CV considérablement. Je souhaite remercier toutes les personnes qui ont participé à la réussite de cette recherche, notamment au comptage microfossile (Philippe Roberge, Camille Brice, Crystal Brochard, Marie-Camille Gasparotto, César Eliès), aux travaux d'analyses (Agnieszka Adamowicz, Jean-François Hélie, Michel Preda, Bassam Ghaleb, Anne de Vernal, Claude Hillaire-Marcel), à la formation/supervision en laboratoire (Maryse Henry, Guillaume Thiery, Sarah Murseli, Carley Crann, Julien Gogot) et finalement tous les membres de l'expédition PS87 pour la collecte et la préparation des échantillons.

Merci à mes parents de m'avoir encouragée à poursuivre des études en Sciences, merci à Emilie Senay, Simon Phaneuf et César

Eliès de m'avoir soutenue et divertie pendant ces trois dernières années et finalement merci à toutes les filles du laboratoire de micropaléontologie pour votre encouragement, vos anecdotes, vos cafés, vos coupes de vin et de gin, vos chalets et jacuzzis et toutes les petites attentions qui ont rendu cette aventure réalisable.

AVANT-PROPOS

La recherche présentée dans ce mémoire porte sur l'étude de six carottes sédimentaires (PS87/023-2, PS87/030-3, PS87/055-1, PS87/070-3, PS87/079-3, PS87/099-4), prélevées lors de l'expédition PS87 à bord du navire de recherche allemand *RV Polarstern* à l'été 2014. Les détails de l'expédition se trouvent dans le rapport d'expédition (Stein, 2015). Dans le cadre de cette étude, le contenu sédimentaire et biogénique de ces carottes a fait l'objet d'analyses minéralogiques, sédimentologiques, palynologiques micropaléontologiques, et géochimiques, conduites à l'UQAM, et de datations au radiocarbone, conduite au laboratoire A.E. Lalonde de l'Université d'Ottawa. L'analyse minéralogique par diffraction aux rayons X a été menée par Michel Preda, l'analyse palynologique des carottes a été réalisée par Anne de Vernal, les analyses géochimiques ont été conduites par Agnieszka Adamowicz avec l'aide de Jean-François Hélie, les datations au radiocarbone, sur l'accélérateur de particules, a été dirigée par le Dr. Xiaolei Zhao et les analyses ^{226}Ra et ^{230}Th ont été faites par Bassam Ghalem.

Le mémoire a été construit autour d'un article scientifique qui sera soumis à la revue *Marine Geology* au courant de l'année 2019. Le contenu de l'article, rédigé en langue originale anglaise suivant les directives de la revue, est présenté dans le Chapitre 1.

TABLE DES MATIÈRES

AVANT-PROPOS	iv
LISTE DES FIGURES	vii
LISTE DES TABLEAUX	viii
LISTE DES ABBRÉVIATIONS DES SIGNES ET DES ACRONYMES ...	ix
LISTE DES SYMBOLES ET DES UNITÉS	xii
RÉSUMÉ	xiv
INTRODUCTION	1
CHAPITRE 1	
CONTRASTED EAST-WEST SEDIMENTARY FLUXES ALONG THE LOMONOSOV RIDGE (ARCTIC OCEAN) DURING THE LATE QUATERNARY	4
ABSTRACT	5
1.1 Introduction	7
1.2 Oceanographic setting of the Lomonosov Ridge	8
1.3 Material and methods	10
1.3.1 Study sites	10
1.3.2 Radiocarbon analysis	10
1.3.3 Carbon and nitrogen analysis.....	11
1.3.4 Sedimentological analysis.....	12
1.3.5 U-series isotopes analysis.....	12
1.4 Results.....	13
1.4.1 Radiocarbon analysis	13
1.4.2 Carbon and nitrogen analysis.....	15
1.4.3 Sedimentological analysis.....	16
1.4.4 U-series isotopes analysis.....	17

1.5 Discussion	18
1.5.1 Nature and origin of sediments	18
1.5.2 Behavior of U-series isotopes	20
1.5.3 Contrasted East-West sedimentary regimes	21
1.6 Conclusion.....	23
1.7 Acknowledgements.....	24
1.8 References	25
CONCLUSION	43
APPENDICE A TABLEAUX DES RÉSULTATS D'ANALYSES	45
APPENDICE B PROCÉDURES DE LABORATOIRE DÉTAILLÉES	58
APPENDICE C COMPARAISON DES RÉSULTATS $\delta^{13}\text{C}$ DE DEUX MÉTHODES DE DÉCARBONISATION : ACIDIFICATION PAR FUMIGATION ET ACIDIFICATION EN SOLUTION.....	62
APPENDICE D DÉNOMBREMENT DE LA MICROFAUNE	64
BIBLIOGRAPHIE.....	72

LISTE DES FIGURES

Figure	Page
1.1 Map of the Arctic Ocean based on the International bathymetric chart of the Arctic Ocean (IBCAO) featuring the location of the study cores along the Lomonosov Ridge.....	36
1.2 Age vs. depth relationship from ^{14}C -AMS measurements of the study cores.....	37
1.3 Age, sedimentological and geochemical properties of the upper 12 cm of the study cores	38
1.4 Lead-210 (blue), Radium-226 (green) and Thorium-230 (red) activities in the upper 12 cm of core PS87/030-3...	39

LISTE DES TABLEAUX

Tableau	Page
1.1 Cores locations and bathymetry	40
1.2 AMS- ¹⁴ C data and calibrated ages of the study cores.....	41

LISTE DES ABBRÉVIATIONS, DES SIGNES ET DES ACRONYMES

AMS	<i>Accelerator mass spectrometry</i> Spectrométrie de masse par accélérateur
AO	<i>Arctic Oscillation</i> Oscillation arctique
AOO	<i>Arctic Ocean Oscillation</i> Oscillation de l'océan Arctique
BP	<i>Before Present</i> Avant l'actuel
C	Carbone
CaCO_3	Carbonate de calcium
cal. yr	Calibrated year Année calibrée
cf.	<i>Confer</i> Se reporter à
Ctot	<i>Total carbon</i> Carbone total
DIMS	Dual inlet mass spectrometry Spectromètre de masse à double système d'introduction
Dr.	Docteur
dw	Dry weight Poids sec

e.g.	<i>Exempli gratia</i> Par exemple
et al.	<i>Et alii</i> Et autres
HCl	Acide chlorhydrique
i.e.	<i>id est</i> C'est-à-dire
IRD	<i>Ice rafted debris</i> Débris de délestage
Lab.	Laboratoire
LGM	<i>Last Glacial Maximum</i> Dernier maximum glaciaire
MC-ICPMS	Multicollector-Inductively Coupled Plasma Mass Spectrometer Spectromètre de masse à plasma inductif
MIS	Marine isotopic stage Stade isotopique marin
N	Nitrogen Azote
Ntot	<i>Total nitrogen</i> Azote total
Pa	Protactinium
Pb	Plomb
PS87	87 ^e expédition du <i>Polarstern</i>
R	Réservoir

Ra	Radium
RV	<i>Research vessel</i> Navire de recherche
TIC/C _{inorg}	<i>Total inorganic carbon</i> Carbone inorganique total
TOC/C _{org}	<i>Total organic carbon</i> Carbone organique total
Th	Thorium
TPD	Transpolar Drift Dérive transpolaire
XRD	Diffraction aux rayons X

LISTE DES SYMBOLES ET DES UNITÉS

%	Pour cent
%o	Pour mille
<	Plus petit que
>	Plus grand que
~	Environ
±	Plus ou moins
δ/Δ	Delta
Φ	Phi
σ	Sigma
°	Degrés
°C	Degrés Celsius
dpm	Désintégrations par minute
μm	Micromètre
cm	Centimètre
g	Gramme
km	Kilomètre
kyr/ka	<i>Kilo years/kilo annum (Thousand years)</i> Millier d'années

m	Mètre
mg	Milligramme
yr	<i>Year</i> Année

RÉSUMÉ

Au cœur de l'océan Arctique se dresse une dorsale sous-marine parcourant plus de 1800 kilomètres depuis les mers de Laptev et de Sibérie orientale jusqu'au nord du Groenland et de l'archipel arctique canadien: la ride de Lomonosov. Située à la confluence des courants de la dérive transpolaire (TPD) et de la gyre de Beaufort, la région se caractérise par une couverture de glace de mer pluriannuelle. L'analyse à haute résolution de 6 carottes prélevées en 2014 lors de l'expédition PS87 du *RV Polarstern* a été entreprise dans le but de caractériser et quantifier la composition ainsi que les flux sédimentaires le long de la ride de Lomonosov à la fin du Quaternaire. Les mesures effectuées incluent des datations au radiocarbone par spectrométrie de masse (AMS) de carbonates biogéniques, une analyse de l'activité des isotopes des séries de l'uranium (Pb-Ra-Th) par comptage alpha (^{210}Pb) et gamma (^{226}Ra) et par MC-ICPMS (^{230}Th), des analyses granulométriques au granulomètre laser, minéralogiques par diffraction au rayons X (XRD), et géochimiques (C, N, $\delta^{13}\text{Corg}$) sur analyseur élémentaire et spectrométrie de masse.

Les résultats d'analyse mettent en relief des régimes sédimentaires fortement contrastés permettant d'identifier deux zones distinctes: l'une marquée par des apports dolomitiques et de très faibles flux sédimentaires à l'ouest de la ride de Lomonosov et l'autre marquée par des flux sédimentaires plus élevés au sud-est de la ride de Lomonosov. L'étude révèle également des bioturbations et une diffusion du ^{226}Ra dans les sédiments de surface, rendant impossible le calcul des flux sédimentaires récents par le biais de la séquence de décroissance radioactive $^{226}\text{Ra}-^{210}\text{Pb}$. L'analyse au radiocarbone fournit ici une estimation des vitesses de sédimentation au cours des derniers ~40 ka, allant de $>30 \text{ mm} \cdot 10^3 \text{ an}^{-1}$ dans le secteur sud-est à $\sim 5.3 \text{ mm} \cdot 10^3 \text{ an}^{-1}$ à l'ouest. Issus principalement du dépôt de débris de délestage transportés par la glace de mer, les sédiments ont enregistré l'histoire glaciaire récente de l'océan Arctique et rendent compte du rôle majeur de la dynamique de glace de mer le long de la ride de Lomonosov.

MOTS-CLÉS: océan Arctique, Lomonosov, Quaternaire, glace de mer

INTRODUCTION

Dans un contexte de réchauffement climatique, affectant l'Arctique plus rapidement et sévèrement que les autres régions de la planète (A.C.I., 2004), le rôle que peut avoir l'océan Arctique dans la régulation du climat global (CliC/AMAP/IASC, 2016), notamment via le couvert de glace et les bilans d'eau douce et donc la circulation thermohaline, revêt une importance considérable. L'un des facteurs déterminant des bilans de chaleur terrestre est l'étendue du couvert de glace de mer. La diminution de l'étendue de glace de mer en Arctique influe sur l'albédo et serait à l'origine de rétroactions positives responsables de l'amplification arctique (Screen and Francis, 2016; Kumar et al., 2010). Bien que l'étendue de glace de mer arctique fasse aujourd'hui l'objet d'un suivi régulier, ses variations avant la période d'observations par satellites restent incertaines. Or, il est possible de retracer l'histoire du transport des sédiments via la dérive des radeaux de glace par l'étude des enregistrements sédimentaires, soit des vitesses de sédimentation et de la provenance des matériaux détritiques, sur le plancher océanique.

Dans cette optique, des études assez récentes portant sur la sédimentation récente au centre de la ride de Lomonosov ont mené à des estimations des vitesses de sédimentation de l'ordre de 1 à 3 cm. 10^3 an $^{-1}$ par le biais de différentes techniques de datation géochronologiques, telles que l'analyse des propriétés physiques des sédiments (Sellén et al., 2010; Jakobsson et al., 2000; O'Regan et al., 2008), la luminescence optique (Jakobsson et al., 2003), l'usage de marqueurs biostratigraphiques (Backman et al., 2004) et

de mesures $^{10}\text{Be}/^{9}\text{Be}$ (Backman et al., 2008; Frank et al., 2008). Des études antérieures, dans des régions voisines, ont livré des estimations plus faibles de 0,2 à 0,3 mm. 10^3 an $^{-1}$ sur la base de mesures du thorium-230 (Cranston, 1997; Huh et al., 1997) variant de 1.5 à 3 mm. 10^{-3} sur la ride de Mendéléïev (Figure 1.1) à partir de l'analyse de radionucléides naturels (^{210}Pb , ^{226}Ra et ^{230}Th ; Not et al., 2008; 2010). Bien que ces études révèlent d'importantes disparités, selon les approches méthodologiques utilisées, il est important de s'attarder aux différences régionales liées à l'hydrographie et aux trajectoires des radeaux de glace via les courants, lesquels pourraient être à l'origine des écarts observés.

Située au centre de l'océan Arctique et soumise à l'action d'importants courants de surface, tels que la dérive transpolaire (TPD) et la gyre de Beaufort, la ride de Lomonosov occupe une situation stratégique pour l'étude de la dynamique de la glace de mer. Afin de mesurer les flux sédimentaires récents le long de la ride de Lomonosov et ainsi de retracer l'étendue du couvert de glace, l'étude détaillée de six carottes sédimentaires prélevées au cours de l'expédition PS87 à bord du *RV Polarstern* (Stein et al., 2015) a été entreprise. Les sites d'étude (Tableau 1.1) sont situés le long d'un transect allant de l'ouest (Nord du Groenland) vers l'est (Mer de Laptev) sous une couverture de glace de mer pérenne, selon le recensement sur l'étendue médiane de septembre de 1979-2000 (NSIDC, 2012a). Cependant, le secteur est de la zone d'étude a été marqué, de façon exceptionnelle, par des conditions océaniques libres de glace en septembre, en 2007 et 2012 (NSIDC, 2012b).

Dans le cadre de mon travail de maîtrise, des analyses granulométriques, minéralogiques, sédimentaires et géochimiques (C, N, $\delta^{13}\text{C}$) ont été menées afin d'évaluer la nature et l'origine des sédiments et d'améliorer les

connaissances en ce qui a trait à la dynamique de la glace de mer dans l'océan Arctique au cours des derniers milliers d'années. De plus, des profils ^{210}Pb et ^{14}C ont été dressés afin d'estimer les flux sédimentaires. L'article qui suit présente les résultats d'analyses ainsi que les conclusions obtenues au terme de cette recherche.

CHAPITRE 1

CONTRASTED EAST-WEST SEDIMENTARY REGIMES ALONG THE LOMONOSOV RIDGE (ARCTIC OCEAN) DURING THE LATE QUATERNARY

Cynthia Le Duc¹, Anne de Vernal¹, Claude Hillaire-Marcel¹,
Bassam Ghaleb¹, Robert F. Spielhagen² and Ruediger Stein³

¹ GEOTOP-UQAM, CP 8888 Montréal, H3C 3P8, Canada

² GEOMAR Helmholtz Centre for Ocean Research, 24148 Kiel, Germany

³ Alfred Wegener Institute for Polar and Marine Research, Bremerhaven,
Germany

ABSTRACT

We report here on sedimentary and geochemical properties of six short sequences collected during the 2014 *RV Polarstern* expedition PS87 along the Lomonosov Ridge with the objective to characterize and quantify sediment composition and accumulation rates within the ^{14}C -dating range of the late Quaternary. Centimeter-thick samples were collected continuously for the measurement of ^{14}C in biogenic carbonates, wherever available, ^{210}Pb in bulk sediment, as well as grain size, organic vs inorganic carbon and nitrogen contents, and mineralogy. Occurrences of detrital dolomite from the Canadian Arctic Archipelago and Beaufort Sea area characterize low sedimentation rate sequences of the westernmost section of the Ridge, whereas order(s) of magnitude higher deposition rates of siliciclastic sediments are observed in its eastern sector. In the lowest sedimentation rate core from the western sector, the distribution of downcore ^{210}Pb is tightly controlled by bioturbation processes down to ~ 2 cm, then by ^{226}Ra diffusion down to ~ 8 cm downcore, hampering the use of the ^{226}Ra - ^{210}Pb radioactive system for the calculation of recent sedimentation rates. AMS- ^{14}C provide reliable radiometric ages below the mixed layer. First order estimates of sedimentation rates during the last ~ 40 kyr, range from > 30 mm.kyr $^{-1}$ in the easternmost sector, to ~ 5.3 mm.kyr $^{-1}$ westward, hence illustrating more than one order of magnitude difference in accumulation rates, mostly linked to ice-rafting deposition by the Trans-Polar Drift, along the Ridge. Cores spanning the Last Glacial Maximum depict a sedimentary gap during this interval, as generally observed in low sedimentation rate sites of the central Arctic Ocean. Combining sedimentological and

geochemical features, one may infer a major role of sea ice dynamics over the Ridge.

Keywords: Arctic Ocean, Lomonosov Ridge, Quaternary, Sea-Ice

1.1. Introduction

Located in the middle of the Arctic Ocean, the Lomonosov Ridge represents one of the sites where complex sea-ice dynamics and deep-water exchanges affect the global oceanic circulation (McPhee et al., 2009; Björk et al., 2007). The analysis of sedimentary sequences from the Lomonosov Ridge may thus help assessing sediment transport and sea-ice regime changes through time, and documenting their linkage with the Earth's climate and polar amplification (Screen and Francis, 2016; Kumar et al., 2010).

Recent studies of Quaternary sediments from the central part of the Lomonosov Ridge provided estimate of sedimentation rates in the order of 1-3 cm.kyr⁻¹ using different geochronological approaches such as the analysis of sediment physical properties (Sellén et al., 2010; Jakobsson et al., 2000; O'Regan et al., 2008), luminescence (Jakobsson et al., 2003), biostratigraphic markers (Backman et al., 2004), and ¹⁰Be/⁹Be age models (Backman et al., 2008; Frank et al., 2008). Other studies in nearby regions estimated rates ranging from 0.2-0.3 mm.kyr⁻¹ in the Amerasian Basin (Figure 1.1) based on thorium-230 and pore water chemistry methods (Cranston, 1997; Huh et al., 1997), 1.5-3 mm.kyr⁻¹ on the Mendeleev Ridge (Not et al., 2008, 2010), and ~ 4.3 mm.kyr⁻¹ on the central Lomonosov Ridge (Hillaire-Marcel et al., 2018) (Figure 1.1) using age models based on the decay of excesses in natural radionuclides (²¹⁰Pb, ²³⁰Th). Although these studies disagree on depositional rates, regional differences linked to hydrographic setting could also play

some role on such discrepancies, thus requiring more exhaustive investigations.

In the aim of documenting the recent sedimentary fluxes along the Lomonosov Ridge, we undertook the study of a series of six cores collected during expedition PS87 of the *RV Polarstern* (Stein et al., 2015). The study sites (Table 1.1) are located along a transect from West, off Greenland, to East in the Laptev Sea. They are mostly located under perennial sea ice according to the September median extent of 1979-2000 (cf. National Snow and Ice Data Center) although the southeasternmost sites of the Laptev Sea have experienced exceptional sea ice-free conditions in 2007 and 2012 (Figure 1.1). Sedimentary analyses along with geochemical analyses were carried out to assess the nature, origin and depositional rates of sediments to better understand the sea ice dynamics in the area during the late Quaternary.

1.2. Oceanographic setting of the Lomonosov Ridge

The Lomonosov Ridge is an underwater ridge of continental crust that stretches East-West at 500 m to >2000 m water depth over 1800 km in the center of the Arctic Ocean (Jakobsson et al., 2012), from the Laptev and East Siberian seas to the Canadian Arctic Archipelago and Northern Greenland (Figure 1.1). It separates the Eurasian basin, connected to the North Atlantic, from the Amerasian basin, where surface waters circulate along the Beaufort Gyre (Figure 1.1). Over the Lomonosov Ridge, the Transpolar Drift (here-after TPD) carries Eurasian detrital material via sea-ice export

from the continental shelf of Russia through the eastern Arctic and Fram Strait (e.g., Maccalli et al., 2018; Hillaire-Marcel et al., 2017; Not & Hillaire-Marcel, 2011). In this large region, the atmospheric circulation patterns, which drive surface ocean currents and sea-ice motion in the Arctic Ocean, are controlled by variations in the strength of the polar vortex and gradients in sea-level pressures. Various modes of atmospheric variability have been described in the Arctic: the Arctic Oscillation (AO; Rigor et al., 2002; Thomas and Wallace, 1998), the more polar-centric Arctic Ocean Oscillation (AOO; Proshutinsky and Johnson, 1997) and the dipole anomaly characterized the development of high and low pressure centers over the Arctic (Wu et al., 2006). The interplay between AO, AOO and dipole anomaly is complex, but these modes of variability are translated into variations in cyclonic and anticyclonic circulation over the Arctic, thus regulating strength and trajectories of the Beaufort Gyre and TPD, which respectively recirculate sea ice in the Arctic and export sea ice to the North Atlantic. In the scheme proposed by Proshutinsky et al. (2002), cold Arctic conditions correspond to a strong anticyclonic circulation (positive AOO) over the Arctic, thus resulting in enhanced size and strength of the Beaufort Gyre, which then reaches the Lomonosov Ridge. In contrast, the cyclonic circulation regime (negative AOO), fostered by low sea-level pressure in the Arctic, is characterized by inflow of warm air from the North Atlantic and accompanied by dominant TPD and southward sea ice export through Fram Strait. Hence, the Lomonosov Ridge is located in a critical center of action for what concerns the Arctic Ocean cyclonic/anticyclonic circulation and sea

ice drift pattern, which in turn play a role on the freshwater budget in the Nordic Seas and North Atlantic thermohaline circulation (e.g., Dickson, 1999).

1.3 Material and methods

1.3.1 Study sites

Box cores and multicores used in the present study are localised in Figure 1.1 and Table 1.1. Box cores were sliced at 1 cm intervals and multicores were sampled by extrusion at 1 cm intervals. All samples were stored in a cold room before being processed.

1.3.2 Radiocarbon analysis

Planktic foraminifer tests of *Neogloboquadrina pachyderma* (Np) were hand-picked in the 150-250 μm fraction for radiocarbon dating at the Accelerator Mass Spectrometry (AMS) facility of the A.E. Lalonde Laboratory at the University of Ottawa. The detection limit of radiocarbon at the A.E. Lalonde AMS laboratory during measurements corresponded to ~ 46 kyr ago. Measurements were made on subsamples containing >10 mg of biogenic carbonate. Results were normalized with respect to the reference material Oxalic II ($\text{F}^{14}\text{C}=1.34$) and the ages were calculated using the Libby ^{14}C half-life of 5568 years. The errors quoted for ^{14}C ages represent one standard deviation (± 1 sigma). A delta R (ΔR) of 440 ± 138 years was applied using reference data from the Canadian Arctic as reported in the marine13 reservoir database (Reimer et al., 2013). Such a ΔR is compatible with the highest values reported by Coulthard et al. (2010) from measurements of recent shells

collected in the Canadian Arctic, but it is lower than what proposed Hanslik et al. (2010) based on correlations in Arctic cores. The calibration to calendar ages was performed using the OxCal v4.2.4 software (Ramsey, 2009). The results are reported in Figure 1.2 and Table 1.2 with a 95% confidence interval (2 sigma). Mean sedimentation rate estimates were obtained using linear interpolation between calibrated ^{14}C ages.

1.3.3 Carbon and nitrogen analyses

The carbon (organic and inorganic) and nitrogen contents were measured on dried bulk sediments at 1 cm intervals in the upper 12 cm of all study cores to document recent changes in biogenic fluxes. The total carbon and total nitrogen concentrations were measured on untreated samples with a Carlo ErbaTM NC 2500 elemental analyzer. Results for total carbon (C_{tot}), total nitrogen (N_{tot}), carbonates (CaCO_3), total inorganic carbon (TIC), and total organic carbon (TOC), are expressed in dry weight percent (dw%) of the total sediment. Organic carbon concentrations were obtained using High Temperature Catalytic Combustion analysis (Hélie, 2009). Inorganic carbon was removed through a decarbonation process using two methods: by acidification through fumigation (for all samples), and by acidification in solution (for samples of cores PS87/023-2, PS87/030-3, and PS87/055-1; see Appendix B and C). $\delta^{13}\text{C}_{\text{org}}$ measurements were obtained by analyzing the acidified samples on a Vario MICRO cubeTM elemental analyser coupled with an IsoprimeTM 100 mass spectrometer. $\delta^{13}\text{C}_{\text{org}}$ values are expressed in ‰ vs VPDB (Appendix A; Table A4, cf. Figure 1.3).

The overall reproducibility is $\pm 0,1\%$ or better (1 sigma), based on replicate measurements of carbonate reference materials.

1.3.4 Sedimentological analysis

Grain size analysis was performed on 1 cm-thick samples in the upper 12 cm of all study cores as a first assessment of detrital supply sources and depositional mechanisms (see appendix B for detailed laboratory procedures). Results for mean grain size, clay and sand percentages are shown in Appendix A (Table A1) and Figure 1.3. Moreover, in the aim of characterizing the nature of detrital inputs and identifying their source, the mineralogical composition was determined by x-ray diffraction from bulk ground dried sediments of samples from the upper 12 cm of all cores. Proportions of the main constituents (clinochlore, kaolinite, muscovite, quartz, calcite, Mg-Ca, dolomite and halite) were obtained using softwares Eva and Topas following the Rietveld method (Rietveld, 1969). Results are shown in Appendix A (Table A3).

1.3.5 U-series isotope analysis

For an evaluation of the depth of the biological mixing layer and to help characterizing sedimentation rates, lead-210 activities were measured in samples from the upper 12 cm of all study cores. This was done by alpha counting based on activities of the ^{210}Pb -daughter isotope, ^{210}Po . Complementary measurements were also made in the upper 12 cm of core PS87/030-3 (cf. also Hillaire-Marcel et al., 2017). They include Radium-226 activities, measured

in aliquot samples by gamma spectroscopy, and Thorium-230 excess measurements, as described in Hillaire-Marcel et al. (2017). Analytic reproducibility for all U-series analyses was $\sim 2\%$ based on replicate measurements of the standard. All results are shown in Appendix A (Table A2).

1.4. Results

1.4.1 Radiocarbon analysis

Radiocarbon analyses were performed every 1-2 cm when enough dating material was available (see figure 1.2; table 1.2). Cores PS87/030-3, PS87/079-3 and PS87/099-4 showed disappearance of foraminifers at 16 cm, 17 cm, and 13 cm respectively, below which no biogenic carbonate was available for dating. Core PS87/070-3 exhibited a progressive decrease in concentrations of foraminifers below 20 cm. Overall, the ^{14}C age of surface sediments ranges from 1421 ± 66 years BP in core PS87/099-4 on the southeastern Lomonosov Ridge to 7792 ± 59 years BP in core PS87/030-3 on the western Lomonosov Ridge, thus providing a first estimate for the age of the mixed layer and relative sedimentation rates. In cores PS87/030-3, PS87/055-1, and PS87/070-3, there are some reversals from surface to sub-subsurface, a feature not unusual with biological mixing (e.g., Srdoc et al., 1986).

In core PS87/023-2, the oldest dates of ~ 36.5 kyr BP between 10 and 17 cm may point towards high accumulation rates, but they should be interpreted with caution as they are close to the reliability

limit of ^{14}C ages on marine biogenic carbonates, due to possible secondary calcite precipitation (e.g., Silverberg et al., 2000). Between 16.5 and 8.5 cm, dates of 36.5 to 26.5 kyr BP indicate sedimentation rates averaging 8 mm.kyr^{-1} . Above, at 8.5 and 7.5 cm, ages of 26.5 and 16.5 kyr BP respectively suggest very low sedimentation rates during the marine isotope stage (MIS) 2 dated of 29-14 ka BP (Lisiecki and Raymo, 2005). It could also be a sedimentary hiatus as documented by Not and Hillaire-Marcel (2010) in a core from the Mendeleev Ridge. Finally, from 7.5 cm to the top of the core, the ^{14}C ages led to calculate a sedimentation rate of $\sim 6 \text{ mm.kyr}^{-1}$ (Figure 1.2; Table 1.2).

In cores PS87/030-3 and PS87/055-1, the ages suggest low sedimentation rate throughout the sequence, averaging $\sim 6 \text{ mm.kyr}^{-1}$ and $\sim 5.3 \text{ mm.kyr}^{-1}$ respectively. In core PS87/055-1, an age reversal at 12.5 cm seems to be an anomaly, possibly due to some "non-local mixing" (e.g., Smith et al., 1986). In core PS87/030-3, an age reversal at 12.5 cm with a date of about 25 kyr BP suggests variations in the sedimentary regime from MIS 3 to MIS 2.

On the southeastern side of the Ridge, radiocarbon data in cores PS87/070-3, PS87/079-3 and PS87/099-4 shows much higher sedimentation rates. At the base of core PS87/070-3, from 32 to 26 cm, ages around 12 kyr BP are recorded, which can suggest high accumulation rates during an interval corresponding with the end of the Younger Dryas or vertical mixing of foraminifers over a few

centimeters. Above 13 cm, an average sedimentation rate of 28 mm.kyr⁻¹ can be calculated. The ages in core PS87/079-3 also indicate high sedimentation rates averaging 34.6 mm.kyr⁻¹. Finally, the ages obtained in the upper part of the easternmost core PS87/099-4 show sedimentation rates of the order of 5-10 cm.kyr⁻¹. The apparent increase of sedimentation rates towards the surface can be related to biological mixing (see also ²¹⁰Pb data in section 1.4.4).

1.4.2 Carbon and nitrogen analyses

The results from the first decarbonation method of acidification by fumigation performed on bulk sediments show $\delta^{13}\text{C}_{\text{org}}$ values ranging from -23.55‰ to as high as -2.86‰ in the westernmost cores (PS87/023-2; PS87/030-3; PS87/055-1). The unusually high values for this region are likely due to the presence of dolomite-rich carbonates, which are more resistant to acidification, as shown by the mineralogical analysis (Appendix A; Table A3). A second decarbonation method, using acidification in solution, was thus used to measure the $\delta^{13}\text{C}_{\text{org}}$ and organic carbon content of those samples (see Appendix C). The second analysis yielded a maximum of -21.91‰ for $\delta^{13}\text{C}_{\text{org}}$ (cf. figure 1.3) and TOC values varying from 0.17 to 0.85%. A slight increase in organic carbon, which could be linked to diagenesis, is noticeable towards the surface at all sites. Along the Ridge, N_{tot} values vary from 0.03% to 0.13% with an average of 0.08% (cf. Appendix A; Table A4), falling within the range reported by Schubert and Calvert (2000) in a study on nitrogen from sediments in the region of the Lomonosov Ridge and

Makarov Basin. C/N weighted ratios range from 4.97 to 9.57 with an average of 6.98 and an increasing trend towards the surface at all sites (Figure 1.3 and Appendix A; Table A4). However, as pointed out by Schubert and Calvert (2000), corrections could be applied to C/N ratios by using N_{org} (not measured in this study) rather than N_{tot} values in order to avoid possible misinterpretation of OM sources caused by the presence of inorganic nitrogen bound in clay minerals. The $\delta^{13}\text{C}_{org}$ values vary from -23.9‰ to -21.9‰ with a trend towards higher ^{13}C values at core top of westernmost sites PS87/023-2, PS87/030-3 and PS87/055-1 (Figure 1.3 and Appendix A; Table A4), suggesting higher proportion of marine organic input (Muzuka and Hillaire-Marcel, 1999; Schubert et al. 2000) towards recent time. In contrast to the western sector of the Lomonosov Ridge, the easternmost cores PS87/070-3, PS87/079-3 and PS87/099-4 record relatively high and uniform $\delta^{13}\text{C}_{org}$ values throughout the sequences. This can be explained by the relatively high sedimentation rates of recent sediment, as well as isotope equilibrium of cold surface ocean waters with atmospheric CO₂ (Matthies et al., 2004; Broecker and Maier-Reimer 1992) due to the increased carbon exchanges at the ocean-atmosphere interface during seasonally ice-free episodes.

1.4.3 Sedimentological analysis

As shown in Figure 1.3, the Lomonosov Ridge sediments are dominated by fine particles (~80% silt and ~16% clay versus ~4% sand) yielding a mean grain size of 7.32 µm and a rather uniform grain size downcore, except in cores PS87/030-3 and PS87/055-1.

Sediments from the western sites PS87/023, PS87/030 and PS87/055 show a much higher calcite-rich ($18.05 \pm 7.7\%$) and dolomite-rich ($3.4 \pm 2.0\%$) content than the southeastern sites PS87/070, PS87/079 and PS87/099 ($4.94 \pm 2.9\%$ in calcite and $1.13 \pm 0.5\%$ in dolomite). The easternmost core PS87/099-4 also yielded an average of $73.77 \pm 4.0\%$ in quartz content against $51.82 \pm 7.4\%$ for the western sector (cf. Appendix A; Table A3).

1.4.4 U-series isotopes analysis

Given the detection limit of ^{14}C dating and slow sedimentation processes in the central Arctic Ocean, U-series isotopes (^{210}Pb , ^{226}Ra , ^{230}Th) can be very useful. Not et al. (2008) showed that ^{210}Pb distribution could be used as chronostratigraphical tool in environments marked by low sedimentation rates whereas ^{230}Th excesses ($^{230}\text{Th}_{\text{xs}}$) could provide temporal benchmarks for sedimentary events such as glacial/interglacial periods. For this purpose, the downcore distribution of lead-210 and its parents, radium-226 and thorium-230, were measured in core PS87/030-3. Figure 1.4 exhibits an excess in ^{210}Pb of 10.074 ± 0.358 dpm/g at core top caused by diffusion, mixing and/or bioturbation at the sediment-water interface. The profile then shows a decrease trend of $^{210}\text{Pb}_{\text{xs}}$ down to 2.5 cm linked to its return to equilibrium with parent ^{226}Ra , followed by a reverse increasing trend, down to 6.5 cm, as a result from the upward diffusion gradient of ^{226}Ra , as reported in other Arctic sediments studies (Not et al., 2008; Clough et al., 1997; Huh et al., 1997; Smith et al., 2003). Below, ^{210}Pb distribution follows ^{226}Ra distribution, which is supported by $^{230}\text{Th}_{\text{xs}}$.

A very similar profile was observed in core HLY0503-11 from the Mendeleev Ridge, although the two cores were collected in different areas and at a roughly 1300 meters of water depth difference. This means that the two cores were likely subjected to very similar vertical particle fluxes and sedimentological regimes.

1.5. Discussion

1.5.1 Nature and origin of sediments

In the Arctic Ocean, where ice-rafting and atmospheric dust fallout constitute the main sedimentation processes (Clark, 1982; Mullen et al., 1972), coarse particles are associated with sea ice and/or iceberg deposition (Clark and Hanson, 1983; Lisitzin 2002). Coarse-grained particle contents are often used to distinguish glacial from interglacial sedimentary units (O'Regan et al., 2014) as well as transport modes (O'Regan et al., 2008; Polyak et al., 2010). For instance, size fractions $>250 \mu\text{m}$, are generally linked to iceberg transport (Darby et al., 2006), whereas low concentrations of coarse-grained material in Holocene sediments from the Arctic Ocean have been attributed to sea ice transport (Nørgaard-Pedersen et al., 1998; Darby et al., 2002). In this study, however, limited variation in the coarse fraction is noticeable, in contrast to what has been observed prior to what was assigned to MIS6/7 in longer sediment records of the Lomonosov Ridge (Jakobsson et al., 2001; Spielhagen et al., 2004; O'Regan et al., 2010).

The mineralogical composition may provide insight on the sources of detrital material. Along the TPD trajectory, sediments are

essentially composed of quartz, exported from the Eurasian margin via sea ice, while dolomite-rich carbonates originating from the Canadian margins (Bischof et al., 1996; Philipps and Grantz, 2001) can be associated with transport of material through the Beaufort Gyre (Yamamoto et al., 2017). Such pulses of detrital carbonates were reported from studies of Lomonosov and Mendeleev Ridges sediments (Not & Hillaire-Marcel, 2010; 2012). They have been linked to the export of glacial and/or lacustrine sediments from the Canadian Arctic bedrock (Polyak et al. 2004; Bischof et al., 1996; Philipps and Grantz, 2001). Hence, the mineralogical content of cores from the western Lomonosov Ridge, which are characterized by the relative abundance of carbonate and dolomite, likely relates to sea ice transport through strong Beaufort Gyre.

The micropaleontological content of the sediment consists in abundant biogenic carbonate remains, dominated by planktic and benthic foraminifers and ostracods (Stein, 2015). However, although concentrations are relatively high in some samples, reaching values in the order of 10^3 foraminiferal shells per g (Zwick, 2014; Brice, 2015; cf. Appendix D), the fluxes estimated from sediment accumulation rates are very low flux, in the order of one foraminifer shell per $\text{cm}^2 \text{ yr}^{-1}$ or less and about one ostracod valve per $\text{cm}^2 \cdot 100 \text{ yr}^{-1}$ in the central part of the Lomonosov Ridge. The input of biogenic particles in the Arctic Ocean can originate from pelagic fluxes, ice-rafting, and lateral fluxes as suggested by Fahl and Nöthig (2007) in a study on the easternmost portion of the Ridge, near the Laptev Sea continental margin, using sediment traps. Besides demonstrating low biogenic fluxes in Arctic

sediments, even during sea ice-free months, the study indicates that ocean currents, including turbidity currents and Siberian rivers such as the Lena River, have a significant impact on sedimentary and chemical budgets of the Arctic Ocean via sea ice transport (Eicken et al., 1997, 2000; Holmes et al., 2002; Stein and Fahl, 2004). Sediment transport with sea ice is probably responsible for a part of the biogenic fluxes. However, the biogenic content of sediment also likely relates to regional heterotrophic productivity, although very low, in the water column and the sediment (Wollenburg and Mackensen, 1998). In this study, the unusual abundance of macropaleontological remains found in surface sediments, and the poor preservation state of many of them (Stein 2015; Le Duc et al., 2016) seems consistent with a lateral transport hypothesis.

1.5.2 Behavior of U-series isotopes

The geochemical analyses carried out on core PS87/030-3 show that in low-sedimentation rate environments such as that of the Lomonosov Ridge, which is strongly influenced by mixing and diffusion, the decay sequence ^{226}Ra - ^{210}Pb cannot be used for the calculation of recent sedimentation rates. Deeper in the sedimentary sequence however, the tracking of ^{231}Pa - and ^{230}Th -excesses could potentially provide chronological constraints of respectively ~ 140 ka and ~ 300 ka (Hillaire-Marcel, 2017; Guzev et al., 2012; Not and Hillaire-Marcel, 2012).

1.5.3 Contrasted East-West sedimentary regimes

Although biases in sedimentation rate estimates from ^{14}C ages cannot be discarded due to benthic mixing as well as partial diagenetic dissolution of foraminifer tests (Barber et al., 2007), radiocarbon data remain the most reliable dating method for the last tens of thousands of years in low sedimentation environments. Regardless uncertainties, average sedimentation rates estimated from ^{14}C dating (cf. Figure 1.2; Table 1.2) range from $> 30 \text{ mm.kyr}^{-1}$ in the southeastern sector of the Ridge to $\sim 5.3 \text{ mm.kyr}^{-1}$ westward, demonstrating contrasted East-West sedimentary regimes of at least one order of magnitude. An East-West difference is also discernible in the mineralogy composition of sediment, ranging from quartz-dominated material in the East to carbonate-rich supplied material in the West. The contrast in sedimentation rates between the eastern and western sectors of the Lomonosov Ridge thus suggest not only different accumulation rates, but also input of material from different sources and sea ice drift trajectories. The higher detrital carbonate content in the western part of the Ridge is consistent with inputs from the western Canadian Arctic, therefore indicating transport with sea ice drifting under the dominant influence of the strong Beaufort Gyre. Because the Beaufort Gyre is also responsible for recirculating sea ice in the Arctic and considering drift times of several years from the source area (e.g. Bischof et al., 1996; Philipps and Grantz, 2001) to the coring sites, our data are consistent with occurrence of multiyear sea ice in the western area of the Lomonosov Ridge over the last tens of thousands of years. Perennial sea ice is compatible with

very low sedimentation rates and would explain the biogenic content of sediments, which are totally barren in phytoplanktonic remains suggesting nil primary productivity (de Vernal et al., 2017).

Eastward, close to the Laptev Sea, relatively high sedimentation rates suggest a more dynamical sedimentary regime likely related to sea ice transport and release of particles during the thawing season. Hence, they suggest at least occasional seasonally ice-free conditions and active transport of particles entrained by sea ice and originating from sources such as Siberian rivers and groundwater discharge, coastal erosion, and aeolian material fluxes (Rachold et al., 2004). In the western part of the Lomonosov Ridge, ^{14}C results of core PS87/023-2 suggest a shift from a glacial (almost no sedimentation) to postglacial (low sedimentation) environment. The interval between 8.5 and 7.5 cm, dated of 26.5-16.5 kyr BP indicate a significant decrease in sedimentary fluxes, likely corresponding to almost nil sedimentary inputs during the LGM, likely due to dense ice cover locking the Arctic Ocean. This interval is followed by an increase in sedimentation rates which can be associated with high detrital input during the deglaciation of circum-Arctic regions. Hence, following the LGM, sedimentation along the Ridge was tightly controlled by ice sheet dynamics (Not and Hillaire-Marcel, 2012; O'Regan et al., 2010, Polyak et al., 2010), leading to lower sedimentation in perennial sea ice environments and higher sedimentation in regions marked by

seasonally ice-free episodes, notably in the southeastern sector of the Lomonosov Ridge.

1.6 Conclusion

Despite considerable development in dating methods and improvement in calibration of marine sediments-derived ages in recent years, a debate remained regarding the sedimentary fluxes in the Arctic Ocean. Using sedimentological, geochemical and radio-isotopic analyses, the study presented here demonstrates contrasted sedimentary regimes along the Lomonosov Ridge during the late Quaternary that reveal a strong regionalism. The study also documents different sources of sedimentary particles that allow tracking of sea ice drift patterns responsible for the dispersal of detrital particles. The eastern part of the Lomonosov Ridge, under TPD influence, depicts a sedimentary regime marked by moderately high accumulation rates, which suggests seasonally ice-free episodes. Conversely, the western part of the Ridge, characterized by dolomite-rich carbonates from the Canadian Arctic, exhibits a rather passive regime with extremely low sedimentation rates corresponding to perennial sea ice cover. The sedimentological approaches used here reveal large scale features in terms of fluxes, sedimentary supplies and linkage with sea ice dynamics. More detailed studies allowing in depth investigations of sedimentary sources using tracers such as clay minerals (e.g. Gamboa et al., 2017; Deschamps et al., 2018), iron oxide (Polyak et al., 2004) and radiogenic isotopes (Maccali et al., 2013) could be the next step to refine the present overview.

Acknowledgements

This study is an ArcTrain contribution. It was supported by the Natural Sciences and Engineering Council (NSERC) of Canada and the *Fond pour la Recherche du Québec-Nature et Technologie* (FRQNT). Special thanks to Bassam Ghaleb for the training on radioisotope analyses, Sarah Murseli and Carley Crann for the training at the Radiocarbon laboratory of the A.E. Lalonde AMS Facility (uOttawa), Agnieszka Adamowicz and Jean-Francois at the stable isotope laboratory of Geotop for leading the geochemistry analyses, Masters students Camille Brice, Philippe Roberge, Crystal Brochard, and Guillaume Thiery at UQAM for helping with microfossils and grain size analyses, Michel Preda at NanoQAM for leading the mineralogy analyses, and PS87 expedition scientists for collecting and preparing the samples.

REFERENCES

- Backman, J., Jakobsson, M., Løvlie, R., Polyak, L., & Febo, L. A. (2004). Is the central Arctic Ocean a sediment starved basin?. *Quaternary Science Reviews*, 23(11-13), 1435-1454. <https://doi.org/10.1016/j.quascirev.2003.12.005>
- Backman, J., Jakobsson, M., Frank, M., Sangiorgi, F., Brinkhuis, H., Stickley, C., ... & Gattacecca, J. (2008). Age model and core-seismic integration for the Cenozoic Arctic Coring Expedition sediments from the Lomonosov Ridge. *Paleoceanography*, 23(1). <https://doi.org/10.1029/2007PA001476>
- Barber, David G., and Robert A. Massom. "The role of sea ice in Arctic and Antarctic polynyas." *Elsevier oceanography series* 74 (2007): 1-54.
- Bischof, J., Clark, D. L., & Vincent, J. S. (1996). Origin of ice-rafted debris: Pleistocene paleoceanography in the western Arctic Ocean. *Paleoceanography*, 11(6), 743-756. <https://doi.org/10.1029/96PA02557>
- Björk, G., Jakobsson, M., Rudels, B., Swift, J. H., Anderson, L., Darby, D. A., ... & Edwards, M. (2007). Bathymetry and deep-water exchange across the central Lomonosov Ridge at 88–89 N. *Deep Sea Research Part I: Oceanographic Research Papers*, 54(8), 1197-1208. <https://doi.org/10.1016/j.dsr.2007.05.010>
- Brice, C (2015). *Rapport préliminaire du stage en micropaleontology de l'été 2015*. Unpublished manuscript
- Broecker, W. S., & Maier-Reimer, E. (1992). The influence of air and sea exchange on the carbon isotope distribution in the sea. *Global Biogeochemical Cycles*, 6(3), 315-320. <https://doi.org/10.1029/92GB01672>

- Clark, D. L. (1982). Origin, nature and world climate effect of Arctic Ocean ice-cover. *Nature*, 300(5890), 321.
<https://doi.org/10.1038/300321a0>
- Clark, D. L., & Hanson, A. (1983). Central Arctic Ocean sediment texture: a key to ice transport mechanisms. In *Glacial-marine sedimentation* (pp. 301-330). Springer, Boston, MA.
https://doi.org/10.1007/978-1-4613-3793-5_7
- Clough, L. M., Ambrose, W. G., Cochran, J. K., Barnes, C., Renaud, P. E., & Aller, R. C. (1997). Infaunal density, biomass and bioturbation in the sediments of the Arctic Ocean. *Deep Sea Research Part II: Topical Studies in Oceanography*, 44(8), 1683-1704.[https://doi.org/10.1016/S0967-0645\(97\)00052-0](https://doi.org/10.1016/S0967-0645(97)00052-0)
- Cranston, R. E. (1997). Organic carbon burial rates across the Arctic Ocean from the 1994 Arctic Ocean Section expedition. *Deep Sea Research Part II: Topical Studies in Oceanography*, 44(8), 1705-1723.[https://doi.org/10.1016/S0967-0645\(97\)00065-9](https://doi.org/10.1016/S0967-0645(97)00065-9)
- Darby, D. A., Bischof, J. F., Spielhagen, R. F., Marshall, S. A., & Herman, S. W. (2002). Arctic ice export events and their potential impact on global climate during the late Pleistocene. *Paleoceanography*, 17(2).
<https://doi.org/10.1029/2001PA000639>
- Darby, D. A., Polyak, L., & Bauch, H. A. (2006). Past glacial and interglacial conditions in the Arctic Ocean and marginal seas - a review. *Progress in Oceanography*, 71(2-4), 129-144.
<https://doi.org/10.1016/j.pocean.2006.09.009>
- Deschamps, Charles-Edouard, Jean-Carlos Montero-Serrano, and Guillaume St-Onge. "Sediment provenance changes in the western Arctic Ocean in response to ice-rafting, sea-level and oceanic circulation variations since the last deglaciation." *Geochemistry, Geophysics, Geosystems* (2018). <https://doi.org/10.1029/2017GC007411>

- De Vernal, A., Le Duc, C., Roberge, P., Brice, C., Brochard, C., Hillaire-Marcel, C. (2017). Late Quaternary sedimentary/biogenic fluxes along the Lomonosov Ridge under sub-perennial to perennial sea-ice. Fifth PAST Gateways International Conference, Fiskebäckskil. Unpublished raw data.
- Dickson, B. (1999). Oceanography: All change in the Arctic. *Nature*, 397(6718), 389.
- Edwards, R. L., Chen, J. H., & Wasserburg, G. J. (1987). ^{238}U / ^{234}U / ^{230}Th / ^{232}Th systematics and the precise measurement of time over the past 500,000 years. *Earth and Planetary Science Letters*, 81(2-3), 175-192. [https://doi.org/10.1016/0012-821X\(87\)90154-3](https://doi.org/10.1016/0012-821X(87)90154-3)
- Eicken, H., Reimnitz, E., Alexandrov, V., Martin, T., Kassens, H., & Viehoff, T. (1997). Sea-ice processes in the Laptev Sea and their importance for sediment export. *Continental Shelf Research*, 17(2), 205-233. [https://doi.org/10.1016/S0278-4343\(96\)00024-6](https://doi.org/10.1016/S0278-4343(96)00024-6)
- Eicken, H., Kolatschek, J., Freitag, J., Lindemann, F., Kassens, H., & Dmitrenko, I. (2000). A key source area and constraints on entrainment for basin-scale sediment transport by Arctic sea ice. *Geophysical Research Letters*, 27(13), 1919-1922. <https://doi.org/10.1029/1999GL011132>
- Fahl, K., & Nöthig, E. M. (2007). Lithogenic and biogenic particle fluxes on the Lomonosov Ridge (central Arctic Ocean) and their relevance for sediment accumulation: Vertical vs. lateral transport. *Deep Sea Research Part I: Oceanographic Research Papers*, 54(8), 1256-1272. <https://doi.org/10.1016/j.dsr.2007.04.014>

- Frank, M., Backman, J., Jakobsson, M., Moran, K., O'Regan, M., King, Haley B. A, Kubik P. W., and & Garbe-Schönberg, D. (2008). Beryllium isotopes in central Arctic Ocean sediments over the past 12.3 million years: Stratigraphic and paleoclimatic implications. *Paleoceanography*, 23(1). <https://doi.org/10.1029/2007PA001478>
- Gamboa, Adriana, et al. "Mineralogical, geochemical, and magnetic signatures of surface sediments from the Canadian Beaufort Shelf and Amundsen Gulf (Canadian Arctic)." *Geochemistry, Geophysics, Geosystems* 18.2 (2017): 488-512. <https://doi.org/10.1002/2016GC006477>
- Gusev, E.A., F.E. Maksimov, V.Yu. Kuznetsov, V.A. Basov, E.S. Novikhina, N.V. Kupriyanova, S.B. Levchenko, and I.E. Zherebtsov (2013), Stratigraphy of Bottom Sediments in the Mendeleev Ridge Area (Arctic Ocean), *Doklady Earth Sciences*, 450, 602–606. <https://doi.org/10.1134/S1028334X13060111>
- Hanslik, Daniela, et al. "Quaternary Arctic Ocean sea ice variations and radiocarbon reservoir age corrections." *Quaternary Science Reviews* 29.25 (2010): 3430-3441. <https://doi.org/10.1016/j.quascirev.2010.06.011>
- Hélie, Jean-François (2009). Elemental and stable isotopic approaches for studying the organic and inorganic carbon components in natural samples. In *IOP Conference Series: Earth and Environmental Science* (Vol. 5, No. 1, p. 012005). IOP Publishing. <https://doi.org/10.1088/1755-1307/5/1/012005>
- Hillaire-Marcel, C., Ghaleb, B., de Vernal, A., Maccalli, J., Cuny, K., Jacobel, A., ... & McManus, J. (2017). A New Chronology of Late Quaternary Sequences From the Central Arctic Ocean Based on "Extinction Ages" of Their Excesses in ^{231}Pa and ^{230}Th . *Geochemistry, Geophysics, Geosystems*, 18(12), 4573-4585. <https://doi.org/10.1002/2017GC007050>

- Holmes, R. M., McClelland, J. W., Peterson, B. J., Shiklomanov, I. A., Shiklomanov, A. I., Zhulidov, A. V., ... & Bobrovitskaya, N. N. (2002). A circumpolar perspective on fluvial sediment flux to the Arctic Ocean. *Global Biogeochemical Cycles*, 16(4). <https://doi.org/10.1029/2001GB001849>
- Huh, C. A., Pisias, N. G., Kelley, J. M., Maiti, T. C., & Grantz, A. (1997). Natural radionuclides and plutonium in sediments from the western Arctic Ocean: sedimentation rates and pathways of radionuclides. *Deep Sea Research Part II: Topical Studies in Oceanography*, 44(8), 1725-1743. [https://doi.org/10.1016/S0967-0645\(97\)00040-4](https://doi.org/10.1016/S0967-0645(97)00040-4)
- Jakobsson, M., Løvlie, R., Al-Hanbali, H., Arnold, E., Backman, J., & Mört, M. (2000). Manganese and color cycles in Arctic Ocean sediments constrain Pleistocene chronology. *Geology*, 28(1), 23-26. [https://doi.org/10.1130/0091-7613\(2000\)28<23:MACCIA>2.0.CO;2](https://doi.org/10.1130/0091-7613(2000)28<23:MACCIA>2.0.CO;2)
- Jakobsson, M., Løvlie, R., Arnold, E. M., Backman, J., Polyak, L., Knutson, J. O., & Musatov, E. (2001). Pleistocene stratigraphy and paleoenvironmental variation from Lomonosov Ridge sediments, central Arctic Ocean. *Global and Planetary change*, 31(1-4), 1-22. [https://doi.org/10.1016/S0921-8181\(01\)00110-2](https://doi.org/10.1016/S0921-8181(01)00110-2)
- Jakobsson, M., Backman, J., Murray, A., & Løvlie, R. (2003). Optically Stimulated Luminescence dating supports central Arctic Ocean cm-scale sedimentation rates. *Geochemistry, Geophysics, Geosystems*, 4(2). <https://doi.org/10.1029/2002GC000423>
- Jakobsson, M., Mayer, L., Coakley, B., Dowdeswell, J. A., Forbes, S., Fridman, B., ... & Schenke, H. W. (2012). The international bathymetric chart of the Arctic Ocean (IBCAO) version 3.0. *Geophysical Research Letters*, 39(12). <https://doi.org/10.1029/2012GL052219>

- Kumar, A., Perlwitz, J., Eischeid, J., Quan, X., Xu, T., Zhang, T. & Wang, W. (2010). Contribution of sea ice loss to Arctic amplification. *Geophysical Research Letters*, 37(21).
<https://doi.org/10.1029/2010GL045022>
- Le Duc, C., de Vernal, A., Archambault, P., Brice, C., & Roberge, P. (2016). "Recent" macrofossil remains from the Lomonosov Ridge, central Arctic Ocean. *Geophysical Research Abstracts* Vol. 18, EGU2016-692.
- Lisiecki, L. E., & Raymo, M. E. (2005). A Pliocene-Pleistocene stack of 57 globally distributed benthic $\delta^{18}\text{O}$ records. *Paleoceanography*, 20(1).
<https://doi.org/10.1029/2004PA001071>
- Lisitzin, A. P. (2002). Lithology and Geochemistry of the Zones of Iceberg Sedimentation. In *Sea-Ice and Iceberg Sedimentation in the Ocean* (pp. 387-431). Springer, Berlin, Heidelberg.
https://doi.org/10.1007/978-3-642-55905-1_13
- Maccali, J., Hillaire-Marcel, C., Carignan, J., & Reisberg, L. C. (2013). Geochemical signatures of sediments documenting Arctic sea-ice and water mass export through Fram Strait since the Last Glacial Maximum. *Quaternary Science Reviews*, 64, 136-151.
<https://doi.org/10.1016/j.quascirev.2012.10.029>
- Matthies, M., Bickert, T., & Paul, A. (2004). Last glacial $d^{13}\text{C}$ distribution and deep-sea circulation in the Atlantic Ocean: A model-data comparison. *The South Atlantic During the Late Quaternary: Material Budget and Current System*.
https://doi.org/10.1007/978-3-642-18917-3_30
- McPhee, M. G., Proshutinsky, A., Morison, J. H., Steele, M., & Alkire, M. B. (2009). Rapid change in freshwater content of the Arctic Ocean. *Geophysical Research Letters*, 36(10).
<https://doi.org/10.1029/2009GL037525>
- Mullen, R. E., Darby, D. A., & Clark, D. L. (1972). Significance of atmospheric dust and ice rafting for Arctic Ocean

- sediment. *Geological Society of America Bulletin*, 83(1), 205-212. [https://doi.org/10.1130/0016-7606\(1972\)83\[205:SOADAI\]2.0.CO;2](https://doi.org/10.1130/0016-7606(1972)83[205:SOADAI]2.0.CO;2)
- Muzuka, A. N., & Hillaire-Marcel, C. (1999). Burial rates of organic matter along the eastern Canadian margin and stable isotope constraints on its origin and diagenetic evolution. *Marine Geology*, 160(3-4), 251-270. [https://doi.org/10.1016/S0025-3227\(99\)00022-5](https://doi.org/10.1016/S0025-3227(99)00022-5)
- Nørgaard-Pedersen, N., Spielhagen, R. F., Thiede, J., & Kassens, H. (1998). Central Arctic surface ocean environment during the past 80,000 years. *Paleoceanography*, 13(2), 193-204. <https://doi.org/10.1029/97PA03409>
- Not, C., Hillaire-Marcel, C., Ghaleb, B., Polyak, L., & Darby, D. (2008). ^{210}Pb - ^{226}Ra - ^{230}Th systematics in very low sedimentation rate sediments from the Mendeleev Ridge (Arctic Ocean). *Canadian Journal of Earth Sciences*, 45(11), 1207-1219. <https://doi.org/10.1139/E08-047>
- Not, C., & Hillaire-Marcel, C. (2010). Time constraints from ^{230}Th and ^{231}Pa data in late Quaternary, low sedimentation rate sequences from the Arctic Ocean: an example from the northern Mendeleev Ridge. *Quaternary Science Reviews*, 29(25), 3665-3675. <https://doi.org/10.1016/j.quascirev.2010.06.042>
- Not, C., & Hillaire-Marcel, C. (2012). Enhanced sea-ice export from the Arctic during the Younger Dryas. *Nature Communications*, 3, 647. <https://doi.org/10.1038/ncomms1658>
- O'Regan, M., King, J., Backman, J., Jakobsson, M., Pälike, H., Moran, K., Heil, C., Sakamoto, T., Cronin, T.M. & Jordan, R. W. (2008). Constraints on the Pleistocene chronology of sediments from the Lomonosov Ridge. *Paleoceanography*, 23(1). <https://doi.org/10.1029/2007PA001551>
- O'Regan, M., Jakobsson, M., & Kirchner, N. (2010). Glacial geological implications of overconsolidated sediments on the

- Lomonosov Ridge and Yermak Plateau. *Quaternary Science Reviews*, 29(25), 3532-3544.
<https://doi.org/10.1016/j.quascirev.2010.09.009>
- O'Regan, M., Sellen, E., & Jakobsson, M. (2014). Middle to late Quaternary grain size variations and sea-ice rafting on the Lomonosov Ridge. *Polar Research*, 33(1), 23672.
<https://doi.org/10.3402/polar.v33.23672>
- Phillips, R. L., & Grantz, A. (2001). Regional variations in provenance and abundance of ice-raftered clasts in Arctic Ocean sediments: implications for the configuration of late Quaternary oceanic and atmospheric circulation in the Arctic. *Marine Geology*, 172(1-2), 91-115.
[https://doi.org/10.1016/S0025-3227\(00\)00101-8](https://doi.org/10.1016/S0025-3227(00)00101-8)
- Polyak, L., Curry, W. B., Darby, D. A., Bischof, J., & Cronin, T. M. (2004). Contrasting glacial/interglacial regimes in the western Arctic Ocean as exemplified by a sedimentary record from the Mendeleev Ridge. *Palaeogeography, Palaeoclimatology, Palaeoecology*, 203(1-2), 73-93.
[https://doi.org/10.1016/S0031-0182\(03\)00661-8](https://doi.org/10.1016/S0031-0182(03)00661-8)
- Polyak, L., Alley, R. B., Andrews, J. T., Brigham-Grette, J., Cronin, T. M., Darby, D. A., ... & Jennings, A. E. (2010). History of sea ice in the Arctic. *Quaternary Science Reviews*, 29(15-16), 1757-1778. <https://doi.org/10.1016/j.quascirev.2010.02.010>
- Proshutinsky, A. Y., & Johnson, M. A. (1997). Two circulation regimes of the wind-driven Arctic Ocean. *Journal of Geophysical Research: Oceans*, 102(C6), 12493-12514.
- Proshutinsky, A., Bourke, R. H., & McLaughlin, F. A. (2002). The role of the Beaufort Gyre in Arctic climate variability: Seasonal to decadal climate scales. *Geophysical Research Letters*, 29(23).
- Rachold, V., Eicken, H., Gordeev, V. V., Grigoriev, M. N., Hubberten, H. W., Lisitzin, A. P., ... & Schirrmeyer, L. (2004). Modern terrigenous organic carbon input to the Arctic Ocean.

- In *The organic carbon cycle in the Arctic Ocean* (pp. 33-55). Springer, Berlin, Heidelberg.
- Ramsey, Christopher Bronk (2009). Bayesian analysis of radiocarbon dates. *Radiocarbon*, 51(1), 337-360. <https://doi.org/10.1017/S003382200033865>
- Reimer, P.J., Bard, E., Bayliss, A., Beck, J.W., Blackwell, P.G., Bronk Ramsey, C., ... & van der Plicht, J. (2013). IntCal13 and MARINE13 radiocarbon age calibration curves 0-50000 years calBP. *Radiocarbon* 55(4), 1869-1887. https://doi.org/10.2458/azu_js_rc.55.16947
- Rietveld, HaM. "A profile refinement method for nuclear and magnetic structures." *Journal of applied Crystallography* 2.2 (1969): 65-71.
- Rigor, I. G., Wallace, J. M., & Colony, R. L. (2002). Response of sea ice to the Arctic Oscillation. *Journal of Climate*, 15(18), 2648-2663. [https://doi.org/10.1175/1520-0442\(2002\)015<2648:ROSITT>2.0.CO;2](https://doi.org/10.1175/1520-0442(2002)015<2648:ROSITT>2.0.CO;2)
- Schubert, C. J., & Calvert, S. E. (2001). Nitrogen and carbon isotopic composition of marine and terrestrial organic matter in Arctic Ocean sediments: implications for nutrient utilization and organic matter composition. *Deep Sea Research Part I: Oceanographic Research Papers*, 48(3), 789-810 [https://doi.org/10.1016/S0967-0637\(00\)00069-8](https://doi.org/10.1016/S0967-0637(00)00069-8)
- Schubert, C. J., Ferdelman, T. G., & Strotmann, B. (2000). Organic matter composition and sulfate reduction rates in sediments off Chile. *Organic Geochemistry*, 31(5), 351-361. [https://doi.org/10.1016/S0146-6380\(00\)00005-X](https://doi.org/10.1016/S0146-6380(00)00005-X)
- Screen, J. A., & Francis, J. A. (2016). Contribution of sea-ice loss to Arctic amplification is regulated by Pacific Ocean decadal variability. *Nature Climate Change*, 6(9), 856. <https://doi.org/10.1038/nclimate3011>

- Sellén, E., O'Regan, M., & Jakobsson, M. (2010). Spatial and temporal Arctic Ocean depositional regimes: a key to the evolution of ice drift and current patterns. *Quaternary Science Reviews*, 29(25-26), 3644-3664.
<https://doi.org/10.1016/j.quascirev.2010.06.005>
- Silverberg, N., Sundby, B., Mucci, A., Zhong, S., Arakaki, T., Hall, P., Landen, A., Tenberg, A., 2000. Remineralization of organic carbon in eastern Canadian margin sediments, *Deep-Sea Res.*, 47, 699-731.
- Smith, John Norton, Bernard P. Boudreau, and Victor Noshkin. "Plutonium and ^{210}Pb distributions in northeast Atlantic sediments: subsurface anomalies caused by non-local mixing." *Earth and Planetary Science Letters* 81.1 (1986): 15-28.
- Smith, J. N., Moran, S. B., & Macdonald, R. W. (2003). Shelf-basin interactions in the Arctic Ocean based on ^{210}Pb and Ra isotope tracer distributions. *Deep Sea Research Part I: Oceanographic Research Papers*, 50(3), 397-416.
[https://doi.org/10.1016/S0967-0637\(02\)001668](https://doi.org/10.1016/S0967-0637(02)001668)
- Spielhagen, R. F., Baumann, K. H., Erlenkeuser, H., Nowaczyk, N. R., Nørgaard-Pedersen, N., Vogt, C., & Weiel, D. (2004). Arctic Ocean deep-sea record of northern Eurasian ice sheet history. *Quaternary Science Reviews*, 23(11), 1455-1483.
<https://doi.org/10.1016/j.quascirev.2003.12.015>
- Srdoč, D., Horvatinčić, N., Obelić, B., Krajcar-Bronić, I., & O'Malley, P. (1986). The effects of contamination of calcareous sediments on their radiocarbon ages. *Radiocarbon*, 28(2A), 510-514.
- Stein, R., & Fahl, K. (2004). The Laptev Sea: distribution, sources, variability and burial of organic carbon. In: Stein, R. and Macdonald, RW (Eds.), *The Organic Carbon Cycle in the Arctic Ocean*. Springer-Verlag, Berlin (pp. 213-237).
<http://hdl.handle.net/10013/epic.19101>

- Stein, R. (2015). The expedition PS87 of the Research Vessel Polarstern to the Arctic Ocean in 2014. Alfred-Wegener-Institut, Helmholtz-Zentrum für Polar- und Meeresforschung. https://doi.org/10.2312/bzpm_0688_2015
- Thompson, D. W., & Wallace, J. M. (1998). The Arctic Oscillation signature in the wintertime geopotential height and temperature fields. *Geophysical research letters*, 25(9), 1297-1300. <https://doi.org/10.1029/98GL00950>
- Wollenburg, J. E., & Mackensen, A. (1998). On the vertical distribution of living (Rose Bengal stained) benthic foraminifers in the Arctic Ocean. *The Journal of Foraminiferal Research*, 28(4), 268-285.
- Wu, B., Wang, J., & Walsh, J. E. (2006). Dipole anomaly in the winter Arctic atmosphere and its association with sea ice motion. *Journal of Climate*, 19(2), 210-225. <https://doi.org/10.1175/JCLI3619.1>
- Yamamoto, M., Nam, S. I., Polyak, L., Kobayashi, D., Suzuki, K., Irino, T., & Shimada, K. (2017). Holocene dynamics in the Bering Strait inflow to the Arctic and the Beaufort Gyre circulation based on sedimentary records from the Chukchi Sea. *Climate of the Past*, 13(9), 1111. <https://doi.org/10.5194/cp-13-1111-2017>
- Zwick, Mike Marcell (2016). *Reconstruction of water mass characteristics on the western Lomonosov Ridge*. Unpublished manuscript.

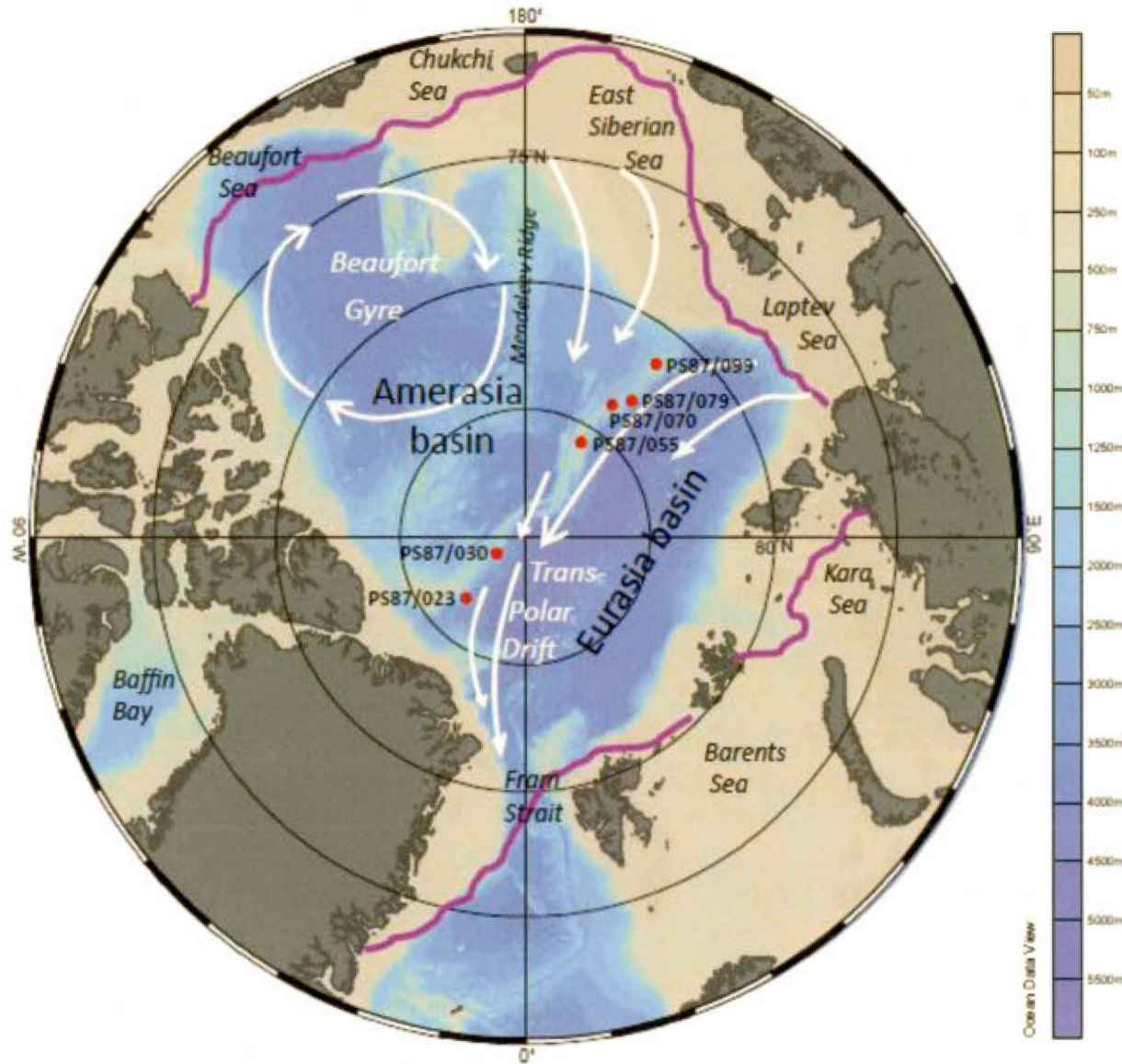


Figure 1.1 Map of the Arctic Ocean based on the International bathymetric chart of the Arctic Ocean (IBCAO) featuring the location of the study cores along the Lomonosov Ridge. The purple line corresponds to the long-term median of the Arctic sea ice extent from 1979 to 2000 (NSIDC, 2012a). The white arrows illustrate the main surface currents: the Beaufort Gyre and the Transpolar Drift.

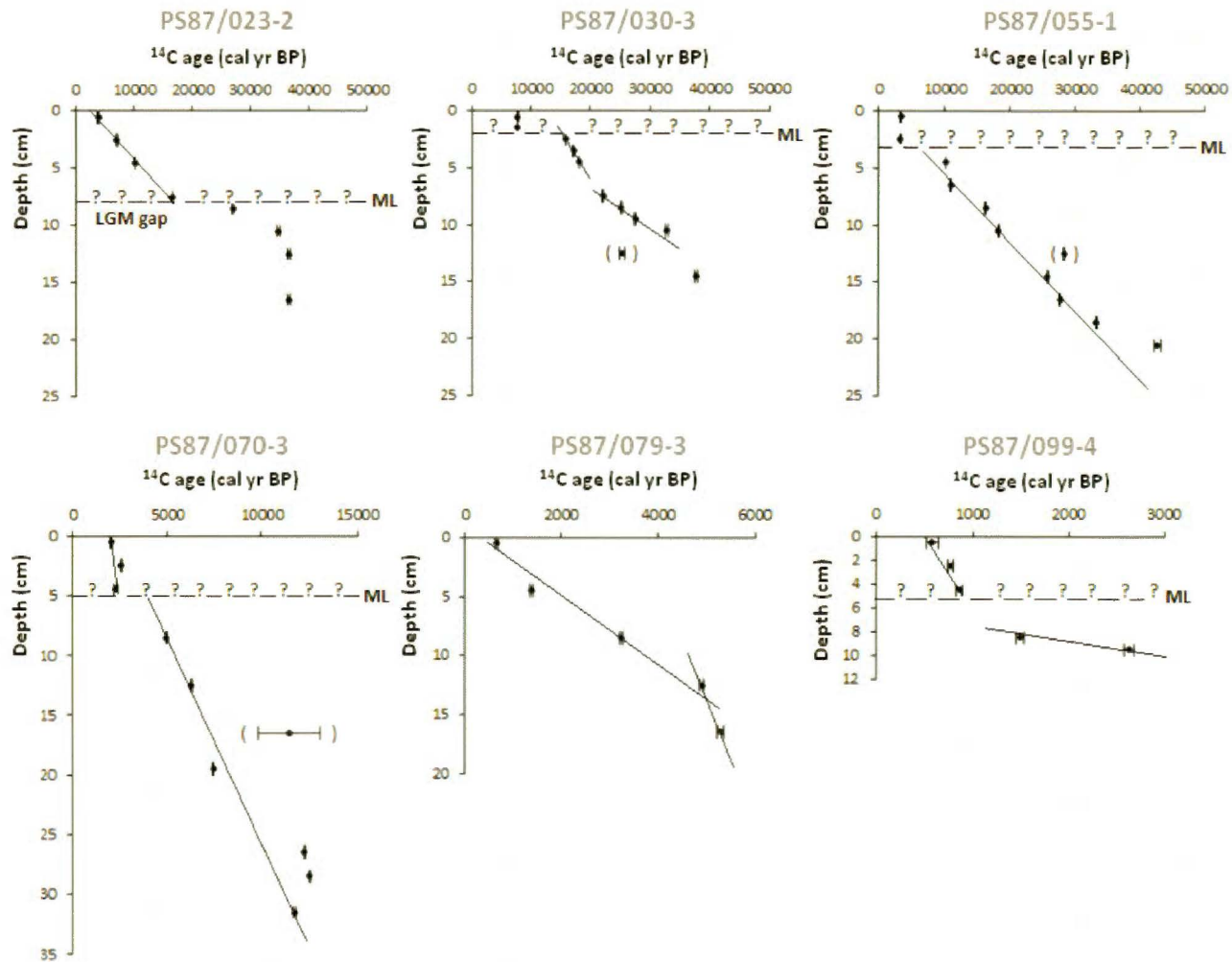


Figure 1.2 Age vs. depth relationship from AMS- ^{14}C measurements, calibration and profiles from the medians of calibrated ^{14}C ages. **ML** = mixed layer, () = outlier discarded from sedimentation rates estimates.



Figure 1.3 Age, sedimentological and geochemical properties of the upper 12 cm of the study cores.

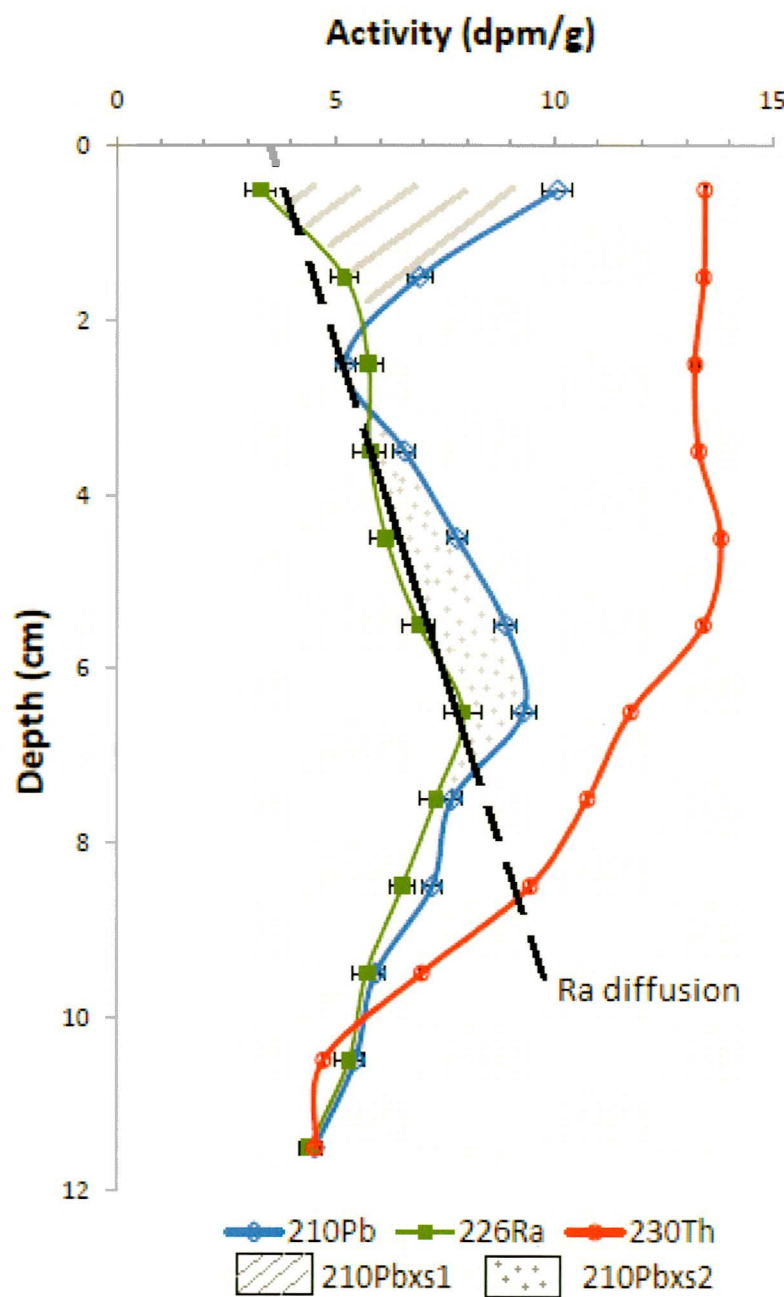


Figure 1.4 Lead-210 (blue), Radium-226 (green) and Thorium-230 (red) activities in the upper 12 cm of core PS87/030-3.
 $^{210}\text{Pb}_{\text{xs}1}$ = excess in ^{210}Pb vs ^{226}Ra due to its scavenging.
 $^{210}\text{Pb}_{\text{xs}2}$ = excess in ^{210}Pb linked to ^{226}Ra diffusion.

Core	Latitude	Longitude	Water depth (m)
PS87/023-2 ^G	86° 37.86' N	44° 52.45' W	2439
PS87/030-3 ^M	88° 39.39' N	61° 25.55' W	1277.8
PS87/055-1 ^G	85° 41.47' N	148° 59.47' E	730.7
PS87/070-3 ^M	83° 48.18' N	146° 7.04' E	1340.2
PS87/079-3 ^M	83° 12.09' N	141° 22.54' E	1358
PS87/099-4 ^M	81° 25.50' N	142° 14.33' E	741.2

Table 1.1 Core locations and bathymetry.
G=Giant box core, **M**=Multi-cores.

Core	Sample depth interval (cm)	Mean depth (cm)	Lab. number	¹⁴ C Age (years BP)	±	Delta R	Median age.	min-max calibrated age (95%)
PS87/023-2	surface	0	UOC-2511	4025	25	440	3486	3135 - 3844
PS87/023-2	0-1	0.5	UOC-1841	4323	66	440	3861	3460 - 4274
PS87/023-2	2-3	2.5	UOC-1842	6976	38	440	7036	6701 - 7344
PS87/023-2	4-5	4.5	UOC-1843	9810	41	440	10202	9765 - 10565
PS87/023-2	7-8	7.5	UOC-2320	14499	60	440	16484	16058 - 16969
PS87/023-2	8-9	8.5	UOC-1844	23025	126	440	26415	26007 - 26975
PS87/023-2	10-11	10.5	UOC-2498	33487	201	440	36618	35887 - 37675
PS87/023-2	12-13	12.5	UOC-1845	33428	266	440	36539	35806 - 37572
PS87/023-2	16-17	16.5	UOC-1846	33423	252	440	36526	35824 - 37520
PS87/030-2	surface	0	UOC-2512	8084	31	440	8108	7826 - 8382
PS87/030-3	0-1	0.5	UOC-1322	7792	59	440	7815	7548 - 8130
PS87/030-3	1-2	1.5	UOC-2321	7636	33	440	7674	7423 - 7933
PS87/030-3	2-3	2.5	UOC-1323	14085	85	440	15900	15348 - 16331
PS87/030-3	3-4	3.5	UOC-2499	16568	63	440	18991	18675 - 19391
PS87/030-3	4-5	4.5	UOC-1324	15700	77	440	18077	17679-18453
PS87/030-3	7-8	7.5	UOC-2322	19110	76	440	22123	21760 - 22460
PS87/030-3	8-9	8.5	UOC-1325	21800	137	440	25273	24642-25707
PS87/030-3	9-10	9.5	UOC-2500	26175	116	440	29389	28889 - 29900
PS87/030-3	10-11	10.5	UOC-2323	29518	219	440	32738	31832 - 33484
PS87/030-3	12-13	12.5	UOC-1326	21998	392	440	25398	24362-26174
PS87/030-3	14-15	14.5	UOC-1327	34341	311	440	37725	36725-38624
PS87/055-1	surface	0	UOC-2513	3643	26	440	3019	2721 - 3354
PS87/055-1	0-1	0.5	UOC-1309	3897	41	440	3324	2946 - 3679
PS87/055-1	2-3	2.5	UOC-2501	5417	28	440	5301	4908 - 5598
PS87/055-1	4-5	4.5	UOC-1310	9819	52	440	10214	9764 - 10580
PS87/055-1	6-7	6.5	UOC-2502	11722	40	440	12779	12553 - 13091
PS87/055-1	8-9	8.5	UOC-1311	14276	124	440	16168	15628 - 16769
PS87/055-1	10-11	10.5	UOC-2503	17559	70	440	20171	19755 - 20559
PS87/055-1	12-13	12.5	UOC-2324	25102	127	440	28288	27876 - 28688
PS87/055-1	14-15	14.5	UOC-2504	22299	83	440	25762	25443 - 26044
PS87/055-1	16-17	16.5	UOC-1313	24321	154	440	27641	27330 - 27949
PS87/055-1	18-19	18.5	UOC-2505	29946	141	440	33318	32806 - 33756
PS87/055-1	20-21	20.5	UOC-1314	39545	525	440	42671	41922 - 43460

PS87/055-1	28-29	28.5	UOC-1315	>46000				
PS87/055-1	36-37	36.5	UOC-1316	>46000				
PS87/070-2	surface	0	UOC-2514	2581	29	440	1729	1389 - 2062
PS87/070-3	0-1	0.5	UOC-1847	2803	29	440	1996	1656 - 2329
PS87/070-3	2-3	2.5	UOC-1848	3273	28	440	2564	2240 - 2900
PS87/070-3	4-5	4.5	UOC-1549	2992	77	440	2225	1863 - 2667
PS87/070-3	8-9	8.5	UOC-1850	5141	36	440	4961	4555 - 5312
PS87/070-3	12-13	12.5	UOC-1851	6288	38	440	6261	5927 - 6570
PS87/070-3	19-20	19.5	UOC-2325	7345	58	440	7409	7122 - 7688
PS87/070-3	26-27	26.5	UOC-2507	11276	39	440	12283	11817 - 12642
PS87/070-3	28-29	28.5	UOC-2508	11528	40	440	12596	12162 - 12890
PS87/070-3	31-32	31.5	UOC-2509	10939	49	440	11689	11199 - 12237
PS87/079-2	surface	0	UOC-2515	1723	24	440	837	597 - 1141
PS87/079-3	0-1	0.5	UOC-2510	1489	21	440	629	413-905
PS87/079-3	4-5	4.5	UOC-1854	2270	26	440	1392	1085 - 1704
PS87/079-3	8-9	8.5	UOC-1855	3848	37	440	3262	2887 - 3605
PS87/079-3	12-13	12.5	UOC-1856	5081	33	440	4878	4507 - 5272
PS87/079-3	16-17	16.5	UOC-2327	5449	64	440	5338	4911 - 5658
PS87/099-3	surface	0	UOC-2516	1171	29	440	356	57 - 570
PS87/099-4	0-1	0.5	UOC-1317	1421	66	440	575	295-853
PS87/099-4	2-3	2.5	UOC-2328	1628	26	440	754	509-1015
PS87/099-4	4-5	4.5	UOC1319	1717	32	440	832	590-1127
PS87/099-4	8-9	8.5	UOC-1320	2335	43	440	1459	1172 - 1796
PS87/099-4	9-10	9.5	UOC-1321	3316	49	440	2611	2275 - 2986

Table 1.2 AMS- ^{14}C data and calibrated ages of the study cores.

CONCLUSION

L'objectif de l'étude était d'identifier la nature et l'origine des particules minérales et de quantifier les flux sédimentaires le long de la ride de Lomonosov afin d'évaluer l'influence du couvert de glace de mer sur les régimes sédimentaires à la fin du Quaternaire. Pour y parvenir, un travail de recherche, comprenant une série d'analyses granulométriques, minéralogiques, sédimentaires et géochimiques, a été effectué. Il inclut notamment le dénombrement de la microfaune, l'identification de la taille et de la nature des minéraux présents dans les sédiments, la datation des carottes sédimentaires, l'identification de la zone de mélange causée par les bioturbations, le remaniement des sédiments de surface et la diffusion des éléments radioactifs à l'interface sédiment-eau, ainsi que l'identification de l'origine des sédiments et de leur mode de transport dans l'océan Arctique.

L'étude indique que l'océan Arctique a été caractérisé par des flux sédimentaires très faibles, composés essentiellement de particules grossières détritiques issues d'un transport par la glace de mer. On observe également un contraste entre les secteurs est et ouest de la ride de Lomonosov, basculant d'un régime sédimentaire plus actif à l'est, sans doute à la faveur d'épisodes de glace de mer saisonnière, vers un milieu quasi-inactif à l'ouest en raison d'un couvert de glace de mer pérenne. Par ailleurs, les enregistrements

sédimentaires étudiés permettent de déduire des flux sédimentaires presque nuls pendant le dernier épisode glaciaire correspondant au stade isotopique 2 (MIS 2), laissant supposer que la circulation de surface et le transport sédimentaire dans l'océan Arctique étaient ralentis en raison du développement d'une banquise continue. L'analyse granulométrique et minéralogique a en outre permis d'identifier une composante d'origine canadienne (carbonates) dans les sédiments du secteur ouest de la ride de Lomonosov, suggérant des apports via la gyre de Beaufort, donc un régime atmosphérique anticyclonique dominé par un fort vortex polaire.

Bien que la datation des sédiments représente un défi dans des milieux de faible sédimentation de l'océan Arctique, notamment en raison de mélanges par bioturbation et à la présence variable du matériel biogénique, les analyses ^{14}C réalisées dans le cadre de cette étude fournissent une estimation assez fiable de l'âge des sédiments arctiques récents. Afin de dresser un portrait plus détaillé de la nature des sédiments qui caractérisent la ride de Lomonosov, il serait pertinent toutefois de poursuivre les analyses minéralogiques (XRD) et l'analyse isotopique ^{210}Pb - ^{226}Ra - ^{230}Th sur de plus longues carottes. Des méthodes permettant de retracer précisément les sources sédimentaires telles que l'analyse des oxydes de fer comme traceur (Polyak et al., 2004) et divers isotopes radiogéniques (Maccali et al., 2013) pourraient également être appliquées.

APPENDICE A

TABLEAUX DES RÉSULTATS D'ANALYSES

Tableau A1: Résultats des analyses granulométriques

Tableau A2: Résultats des analyses des isotopes des séries de l'uranium (Pb-Ra-Th)

Tableau A3: Résultats des analyses minéralogiques (XRD)

Tableau A4: Résultats des analyses géochimiques (carbone, azote) et isotopiques ($\delta^{13}\text{C}$)

Tableau A1: Résultats des analyses granulométriques

	Profondeur (cm)	Sable (dw%)	Silt (dw%)	Argile (dw%)	Moyenne ϕ (μm)
PS87/023-2	0.5	1.73	81.42	16.85	4.98
	1.5	1.45	84.70	13.85	5.23
	2.5	0.35	86.19	13.46	5.06
	3.5	1.69	81.01	17.31	5.18
	4.5	1.00	78.17	20.83	4.86
	5.5	0.78	79.83	19.39	4.69
	6.5	0.89	78.09	21.03	4.44
	7.5	0.49	75.13	24.38	4.1
	8.5	0.00	80.47	19.53	4.36
	9.5	3.43	74.39	22.18	5.3
	10.5	3.48	74.03	22.48	5.12
	11.5	2.91	74.64	22.44	5.33
PS87/030-3	0.5	9.29	77.59	13.12	11.63
	1.5	4.72	79.84	15.44	7.69
	2.5	8.06	71.42	20.52	10.49
	3.5	10.38	71.47	18.15	11.44
	4.5	8.15	72.90	18.94	9.5
	5.5	6.83	76.51	16.66	10.55
	6.5	7.03	75.11	17.86	9.9
	7.5	5.89	75.92	18.18	9.13
	8.5	4.19	79.96	15.85	9.12
	9.5	8.47	75.08	16.45	10.93
	10.5	11.74	71.80	16.46	12.74
	11.5	9.16	74.32	16.53	11.52

	Carotte	Profondeur (cm)	Sable (dw%)	Silt (dw%)	Argile (dw%)	Moyenne ϕ (μm)
PS87/055-1		0.5	0.63	0.35	0.02	12.2
		1.5	0.58	0.39	0.03	6.43
		2.5	0.60	0.37	0.02	8.88
		3.5	0.63	0.35	0.02	14.4
		4.5	0.60	0.37	0.03	10.12
		5.5	0.58	0.39	0.03	6.06
		6.5	0.56	0.40	0.04	5.33
		7.5	0.58	0.38	0.03	7.71
		8.5	0.56	0.40	0.04	4.97
		9.5	0.56	0.40	0.04	5.4
PS87/070-3		10.5	0.57	0.40	0.03	5.3
		11.5	0.56	0.40	0.04	5.45
		0.5	0.58	0.39	0.02	5.93
		1.5	0.59	0.39	0.02	6.61
		2.5	0.60	0.38	0.02	7.12
		3.5	0.60	0.38	0.02	7.05
		4.5	0.59	0.38	0.02	6.97
		5.5	0.59	0.39	0.02	6.21
		6.5	0.59	0.39	0.02	6.57
		7.5	0.59	0.38	0.02	7.3

Carotte	Profondeur (cm)	Sable (dw%)	Silt (dw%)	Argile (dw%)	Moyenne ϕ (μm)
PS87/079-3	0.5	1.56	85.11	13.32	6.95
	1.5	0.11	85.63	14.27	5.88
	2.5	1.98	84.93	13.08	6.97
	3.5	1.13	87.61	11.25	7.08
	4.5	1.72	85.11	13.17	6.69
	5.5	1.36	85.32	13.32	6.34
	6.5	1.49	84.10	14.41	6.25
	7.5	2.56	84.44	13.00	6.94
	8.5	1.52	84.25	14.23	6.51
	9.5	3.05	82.86	14.09	7.09
PS87/099-4	10.5	5.64	79.61	14.75	8.11
	11.5	3.81	81.84	14.35	7.18
	0.5	0.61	0.37	0.02	8.5
	1.5	0.61	0.37	0.02	8.25
	2.5	0.59	0.39	0.02	6.28
	3.5	0.60	0.38	0.02	7.55
	4.5	0.59	0.39	0.02	6.35
	5.5	0.61	0.37	0.02	9.54
	6.5	0.58	0.39	0.03	6.1
	7.5	0.59	0.38	0.02	7.25
	8.5	0.58	0.39	0.03	6.33
	9.5	0.60	0.37	0.02	8.64
	10.5	0.59	0.39	0.02	7.33
	11.5	0.59	0.38	0.03	7.83

Tableau A2: Résultats des analyses des isotopes des séries de l'uranium (Pb-Ra-Th)

Carotte	Profondeur (cm)	210Pb (dpm/g)		226Ra (dpm/g)		230Th (dpm/g)	
			$\pm 2\sigma$		$\pm 2\sigma$		$\pm 2\sigma$
PS87/023-2	0.5	7.377	0.243				
	1.5	8.604	0.272				
	2.5	9.568	0.323				
	3.5	9.592	0.307				
	4.5	11.190	0.338				
	5.5	10.186	0.293				
	6.5	11.745	0.382				
	7.5	14.951	0.460				
	8.5	14.353	0.425				
	9.5	14.933	0.436				
	10.5	16.095	0.472				
	11.5	15.327	0.451				
PS87/030-3	0.5	10.074	0.358	3.297	0.317	13.427	0.038
	1.5	6.922	0.271	5.202	0.324	13.408	0.038
	2.5	5.213	0.218	5.757	0.308	13.207	0.090
	3.5	6.581	0.251	5.782	0.355	13.303	0.038
	4.5	7.781	0.241	6.157	0.343	13.813	0.038
	5.5	8.901	0.270	6.914	0.365	13.412	0.038
	6.5	9.316	0.281	7.925	0.425	11.753	0.035
	7.5	7.677	0.241	7.299	0.377	10.768	0.031
	8.5	7.222	0.224	6.539	0.290	9.469	0.030
	9.5	5.925	0.194	5.719	0.313	6.982	0.022
	10.5	5.465	0.241	5.314	0.311	4.735	0.016
	11.5	4.539	0.207	4.417	0.219	4.547	0.016

Carotte	Profondeur (cm)	210Pb (dpm/g)		226Ra (dpm/g)		230Th (dpm/g)	
			± 2σ		± 2σ		± 2σ
PS87/055-1	0.5	8.361	0.331				
	1.5	4.926	0.199				
	2.5	3.271	0.148				
	3.5	3.917	0.174				
	4.5	3.901	0.172				
	5.5	4.381	0.187				
	6.5	5.950	0.243				
	7.5	9.741	0.385				
	8.5	8.744	0.349				
	9.5	6.567	0.269				
	10.5	5.183	0.251				
PS87/070-3	11.5	5.040	0.228				
	0.5	7.844	0.340				
	1.5	11.039	0.495				
	2.5	9.123	0.413				
	3.5	4.935	0.243				
	4.5	5.372	0.258				
	5.5	6.228	0.307				
	6.5	3.584	0.175				
	7.5	5.334	0.242				
	8.5	3.364	0.169				
	9.5	3.746	0.192				
	10.5	4.333	0.216				
	11.5	4.443	0.229				

Carotte	Profondeur (cm)	210Pb (dpm/g)	$\pm 2\sigma$	226Ra (dpm/g)	$\pm 2\sigma$	230Th (dpm/g)	$\pm 2\sigma$
PS87/079-3	0.5	22.797	0.927				
	1.5	11.290	0.506				
	2.5	8.497	0.385				
	3.5	4.554	0.224				
	4.5	4.788	0.230				
	5.5	6.547	0.324				
	6.5	3.441	0.168				
	7.5	3.580	0.182				
	8.5	3.555	0.179				
	9.5	3.598	0.184				
	10.5	3.690	0.184				
	11.5	3.798	0.197				
PS87/099-4	0.5	12.559	0.533				
	1.5	4.212	0.207				
	2.5	7.807	0.365				
	3.5	2.881	0.152				
	4.5	2.831	0.151				
	5.5	3.070	0.160				
	6.5	2.898	0.147				
	7.5	3.611	0.190				
	8.5	2.735	0.144				
	9.5	2.651	0.141				
	10.5	2.393	0.132				
	11.5	2.418	0.135				

Tableau A3: Résultats des analyses minéralogiques (XRD)

Core	Depth (cm)	Clinochlore (%)	Kaolinite (%)	Muscovite (%)	Quartz (%)	Albite (%)	Microline (%)	Calcite (%)	Pyroxene (%)	Dolomite (%)	Halite (%)	Fraction of total sample (%)
PS87/023-2	0.5	6.8	1.8	14.1	58.1	3.6	0.6	11.8	0.9	1.4	0.9	100
	1.5	5.9	5.1	15.6	58.5	2.8	0.5	9.5	1.1	0.8	0.2	100
	2.5	6.2	5.5	11.3	60.9	2.9	0.5	10.9	0.8	0.8	0.2	100
	3.5	5.3	4.4	14.2	63.4	2.4	0.4	8	1	0.7	0.2	100
	4.5	4.8	4.2	12.7	63.2	3.5	0.4	8.1	0.9	1.4	0.8	100
	5.5	5.1	4.5	14.4	58.8	3.7	0.7	8.9	0.8	2.3	0.8	100
	6.5	5.2	4.1	14.8	57.3	3.4	0.6	10.3	1	2.5	0.8	100
	7.5	6.2	4.6	14.7	56.7	3.3	0.8	9.4	1.1	2.6	0.6	100
	8.5	6.6	4.3	13.7	48.3	3.3	0.8	11.6	1	9.8	0.6	100
	9.5	4.8	1.4	18.4	39.5	2.9	0.6	25.9	trace	6.3	0.2	100
	10.5	4.3	1.3	19.2	38.4	2.6	0.6	27.7	trace	5.7	0.2	100
	11.5	4.9	1.5	16.6	37.6	2.9	0.6	26.2	trace	4.4	0.3	95
PS87/030-3	0.5	2.9	1.3	14.7	48.2	2.5	0.5	23.4	trace	4.8	1.7	100
	1.5	2.8	1.4	20.1	50.7	3.9	1.1	15.6	trace	2.9	1.5	100
	2.5	3.1	1.6	20.2	51.5	4.3	1.2	13.7	trace	3.6	0.8	100
	3.5	2.7	1.4	18.1	51.1	3.7	1	16.9	trace	3.5	1.6	100
	4.5	2.6	2.1	15.1	45.7	3.6	0.7	23.2	trace	4.9	2.1	100
	5.5	2.2	1.1	5.1	58.9	3.1	1.1	21.9	trace	4.3	2.3	100
	6.5	1.8	1.1	15.5	53.8	2.7	0.7	19.6	trace	3.6	1.2	100
	7.5	2.1	1	14.2	47.2	2.1	0.9	27.3	trace	3.5	1.7	100
	8.5	2.1	1.4	9.3	48.4	5.9	0.9	26.6	trace	3.6	1.8	100
	9.5	2.2	0.9	9.6	46.1	2.3	0.4	33.8	trace	3	1.7	100
	10.5	2.8	1.8	17.8	48.3	1.9	0.8	21.1	trace	3.6	1.9	100
	11.5	2.5	1.7	14.2	53.2	2.6	0.7	21.8	trace	1.6	1.7	100
PS87/055-1	0.5	3.1	1.8	16.2	60.1	3.6	1.1	12.2	trace	1.6	0.3	100
	1.5	2.9	1.9	16.3	61.3	3	0.9	11.5	trace	1.9	0.3	100
	2.5	3.7	1.6	17.6	56.1	3.9	1.1	14.9	trace	0.7	0.4	100
	3.5	3.1	1.3	14.3	62.2	3.2	0.9	12.3	trace	2.4	0.3	100

PS87/070-3	4.5	2.4	1.6	10.5	72.3	5.1	1.2	5.4	trace	0.8	0.7	100
	5.5	2.9	1.2	13.7	67.5	2.3	0.5	6.9	trace	4.7	0.3	100
	6.5	3.9	1.2	13.6	58.7	4.1	0.6	14.3	trace	3.3	0.3	100
	7.5	5.5	3.5	14.4	46.6	3.1	0.7	23.5	trace	2.5	0.4	100
	8.5	5.4	2.2	12.3	47.2	3.8	0.7	23.4	trace	4.7	0.5	100
	9.5	9	1.9	15.8	57.9	3.3	0.6	7	trace	4.1	0.4	100
	10.5	3.3	1.2	13.9	69.1	3.3	0.6	4.8	trace	3.4	0.4	100
	11.5	2.7	1.5	12.1	69.7	2.6	0.5	7.4	trace	3.2	0.3	100
	0.5	5.7	1.1	5.3	67.6	10.4	1.2	1.3	trace	0.6	6.1	100
	1.5	4.8	1.1	4.2	70.4	8.9	1.3	6.3	trace	1.2	0.9	100
PS87/079-3	2.5	5.9	1.2	4.1	71.9	6.8	1.2	5.3	trace	2.1	0.8	100
	3.5	6.8	1.4	4.4	69.6	7	1.1	5	trace	2	0.8	100
	4.5	6.1	0.9	5.3	70.4	7.9	1.1	5	trace	2	0.8	100
	5.5	4	0.9	4.2	71.1	7.7	1.1	7.9	trace	1.9	0.8	100
	6.5	3.7	0.9	3.9	71.7	9.3	1.2	5.9	trace	1.8	0.7	100
	7.5	4.2	1.3	3.6	74.3	6.9	1.1	5.4	trace	2	0.8	100
	8.5	2.9	1.2	3.3	73.5	9.4	0.8	6.3	trace	0.9	0.9	100
	9.5	5.2	1.3	2.8	71.9	9.2	0.9	5.4	trace	1.8	0.9	100
	10.5	4.1	1.2	3.7	72.7	7	1.3	7.2	trace	1.4	0.7	100
	11.5	3.6	1.1	4.3	73.4	8.5	1.5	4.7	trace	1.5	0.8	100
PS87/099-4	0.5	5.3	1.1	3.3	64.1	4.6	1.9	5.4	1.7	1.6	10.6	100
	1.5	4.2	1	2.3	55.9	9	2.1	6.7	3.1	1.5	13.7	100
	2.5	3.4	1.1	2.2	57.8	8.1	1.9	7	2.4	1.5	14.2	100
	3.5	3.1	1	2	60.9	7.3	2	6.3	2.2	1.4	13.4	100
	4.5	3.2	1	2	62.5	7.5	1.5	10.3	1.6	1.4	8.6	100
	5.5	3.7	1.2	2.1	57.7	8.7	2	8.5	1.8	1.6	12.3	100
	6.5	3.8	1.2	2.7	59.2	7.9	2.1	8.7	1.9	1.7	10.5	100
	7.5	3.6	1.1	2.6	61.1	7.5	2	8.3	1.8	1.6	10.2	100
	8.5	3.1	1	2.2	64.4	7.3	1.7	7	1.5	1.4	9.2	100
	9.5	3.3	1	2.4	65.1	6.8	1.8	7.6	1.6	1.5	8.7	100
PS87/099-4	10.5	3.4	1.1	2	66.2	6.9	1.8	6.3	1.7	1.5	8.9	100
	11.5	3.6	1.1	2.1	64.1	7.3	1.9	6.8	1.7	1.6	9.4	100
	0.5	2.8	1.5	12.7	72.1	4	0.7	4.3	trace	1.6	0.3	100
	1.5	2.9	1.3	11.9	71.9	4.6	1.5	5.1	trace	0.5	0.3	100
PS87/099-4	2.5	3.4	1.9	15.7	68.2	3.2	0.6	2.8	trace	0.2	0.4	96
	3.5	3.3	1.7	15.8	67.8	3.1	0.6	5.9	trace	1.4	0.4	100

	4.5	3.9	2.1	9.8	77.1	3.6	0.7	1.4	trace	0.9	0.5	100
	5.5	2.7	1.4	11.2	76.7	3.8	1.1	1.9	trace	0.9	0.3	100
	6.5	3.9	2.1	11.3	74.3	5.6	0.8	1.6	trace	0.3	0.1	100
	7.5	4.2	2.2	9.8	74.1	5.9	1.6	1.4	trace	0.4	0.4	100
	8.5	4.6	2.5	6.9	75.6	6.4	1.8	1.5	trace	0.2	0.5	100
	9.5	3.2	1.7	8.4	78.3	4.5	1.2	1.2	trace	1.1	0.4	100
	10.5	2.6	1.9	2.1	79.8	9.4	1.9	1.2	trace	0.9	0.2	100
	11.5	3.3	8.7	8.1	69.3	6.3	2.2	1.3	trace	0.4	0.4	100

Tableau A4: Résultats des analyses géochimiques (carbone, azote) et isotopiques ($\delta^{13}\text{C}_{\text{org}}$)

Carotte	Profondeur (cm)	Ntot (%)	Ctot (%)	CaCO3 (%)	TIC (%)	TOC (%)	C/N	$\delta^{13}\text{C}_{\text{F}}\text{ (‰)}$	$\delta^{13}\text{C}_{\text{S}}\text{ (‰)}$
PS87/023-2	0.5	0.12	1.60	6.44	0.77	0.83	8.27	-22.47	-22.49
	1.5	0.10	1.36	5.35	0.64	0.72	8.06	-22.30	-22.55
	2.5	0.09	1.16	4.59	0.55	0.61	7.81	-22.22	-22.65
	3.5	0.08	1.15	4.80	0.58	0.58	7.95	-22.49	-23.08
	4.5	0.08	1.13	4.86	0.58	0.55	8.03	-22.37	-22.98
	5.5	0.07	1.12	5.35	0.64	0.48	7.55	-21.91	-23.26
	6.5	0.07	1.37	7.97	0.96	0.41	7.04	-21.60	-23.69
	7.5	0.06	1.23	7.23	0.87	0.36	6.83	-20.99	-23.53
	8.5	0.05	1.63	11.10	1.33	0.30	6.45	-19.84	-23.10
	9.5	0.04	2.52	18.79	2.25	0.27	7.16	-11.79	-23.82
	10.5	0.05	2.77	21.04	2.53	0.24	5.87	-8.40	-23.19
PS87/030-3	11.5	0.05	3.35	25.95	3.11	0.24	5.80	-6.24	-23.47
	0.5	0.08	2.98	20.83	2.50	0.49	7.44	-10.77	-22.51
	1.5	0.07	2.06	14.47	1.74	0.32	5.75	-12.64	-22.94
	2.5	0.06	1.98	13.69	1.64	0.33	6.44	-11.70	-23.31
	3.5	0.06	1.86	12.31	1.48	0.38	7.91	-12.62	-22.82
	4.5	0.05	1.97	13.90	1.67	0.30	7.02	-9.70	-23.43
	5.5	0.06	2.05	14.86	1.78	0.26	5.56	-7.17	-23.36
	6.5	0.04	2.59	19.82	2.38	0.21	5.53	-5.52	-23.55
	7.5	0.05	2.80	21.67	2.60	0.20	5.13	-4.96	-23.50
	8.5	0.04	3.06	22.48	2.70	0.36	9.57	-4.16	-22.94
	9.5	0.04	3.04	23.83	2.86	0.18	5.61	-3.27	-23.29
	10.5	0.03	3.49	27.69	3.32	0.17	6.07	-2.98	-23.90
	11.5	0.04	2.75	21.24	2.55	0.20	6.31	-5.10	-23.68

Carotte	Profondeur (cm)	Ntot (%)	Ctot (%)	CaCO3 (%)	TIC (%)	TOC (%)	C/N	$\delta^{13}\text{C-f}^{\text{I}}\ (\text{\textperthousand})$	$\delta^{13}\text{C-s}^{\text{I}}\ (\text{\textperthousand})$
PS87/055-1	0.5	0.08	2.34	15.39	1.85	0.49	7.32	-13.64	-22.53
	1.5	0.08	1.25	5.92	0.71	0.54	7.65	-22.28	-22.51
	2.5	0.07	1.16	6.06	0.73	0.43	6.98	-21.58	-22.83
	3.5	0.07	1.34	8.37	1.00	0.34	5.38	-20.67	-22.83
	4.5	0.07	0.87	4.26	0.51	0.35	6.26	-22.98	-23.34
	5.5	0.06	0.98	5.25	0.63	0.35	6.37	-22.06	-23.12
	6.5	0.05	1.42	9.49	1.14	0.28	6.88	-16.87	-23.06
	7.5	0.05	3.61	28.01	3.36	0.25	6.14	-2.86	-23.25
	8.5	0.06	1.93	13.87	1.66	0.27	5.21	-10.64	-22.69
	9.5	0.07	1.25	7.93	0.95	0.29	4.97	-18.74	-23.28
	10.5	0.07	0.99	5.39	0.65	0.34	5.67	-18.88	-23.58
	11.5	0.07	1.03	6.03	0.72	0.31	5.32	-17.70	-23.82
PS87/070-3	0.5	0.11	1.03	8.61	1.03	0.75	7.84	-22.25	
	1.5	0.11	1.00	8.31	1.00	0.75	8.04	-22.14	
	2.5	0.11	0.97	8.07	0.97	0.76	8.08	-21.96	
	3.5	0.11	0.97	8.08	0.97	0.75	7.91	-21.94	
	4.5	0.11	0.95	7.91	0.95	0.73	7.70	-22.00	
	5.5	0.11	0.94	7.82	0.94	0.73	7.90	-21.91	
	6.5	0.09	0.74	6.17	0.74	0.55	7.05	-22.17	
	7.5	0.09	0.76	6.36	0.76	0.57	7.18	-22.14	
	8.5	0.09	0.76	6.35	0.76	0.49	6.61	-22.32	
	9.5	0.09	0.70	5.84	0.70	0.52	7.07	-22.30	
	10.5	0.08	0.69	5.72	0.69	0.51	7.07	-22.30	
	11.5	0.08	0.62	5.15	0.62	0.49	7.08	-22.34	

Carotte	Profondeur (cm)	N _{tot} (%)	C _{tot} (%)	CaCO ₃ (%)	TIC (%)	TOC (%)	C/N	$\delta^{13}\text{C-f}^1$ (‰)	$\delta^{13}\text{C-s}^1$ (‰)
PS87/079-3	0.5	0.13	1.05	8.76	1.05	0.85	7.77	-22.28	
	1.5	0.11	0.90	7.49	0.90	0.76	8.02	-22.13	
	2.5	0.11	0.89	7.43	0.89	0.74	7.64	-22.10	
	3.5	0.10	0.81	6.75	0.81	0.68	7.52	-21.99	
	4.5	0.11	0.83	6.95	0.83	0.72	7.79	-22.12	
	5.5	0.11	0.81	6.73	0.81	0.72	7.93	-22.09	
	6.5	0.10	0.73	6.06	0.73	0.61	7.13	-22.03	
	7.5	0.09	0.72	5.96	0.72	0.56	7.13	-22.12	
	8.5	0.09	0.68	5.65	0.68	0.53	6.91	-22.12	
	9.5	0.09	0.64	5.32	0.64	0.50	6.68	-22.15	
	10.5	0.09	0.59	4.91	0.59	0.49	6.61	-22.18	
PS87/099-4	11.5	0.09	0.58	4.80	0.58	0.48	6.20	-22.30	
	0.5	0.12	1.14	9.50	1.14	0.82	8.18	-22.74	
	1.5	0.11	0.81	6.75	0.81	0.75	7.90	-23.55	
	2.5	0.11	0.78	6.48	0.78	0.73	7.56	-22.60	
	3.5	0.10	0.74	6.14	0.74	0.69	7.93	-22.55	
	4.5	0.10	0.66	5.54	0.66	0.59	6.88	-22.41	
	5.5	0.10	0.59	4.92	0.59	0.56	6.78	-22.49	
	6.5	0.08	0.63	5.24	0.63	0.50	6.98	-22.54	
	7.5	0.09	0.66	5.49	0.66	0.63	7.75	-22.54	
	8.5	0.08	0.56	4.63	0.56	0.55	7.85	-22.57	
	9.5	0.09	0.54	4.47	0.54	0.49	6.18	-22.45	
	10.5	0.09	0.55	4.57	0.55	0.48	6.39	-22.44	
	11.5	0.09	0.48	4.02	0.48	0.45	6.06	-22.45	

¹ $\delta^{13}\text{C-f}$ fait référence à la méthode de décarbonisation par fumigation tandis que $\delta^{13}\text{C-s}$ fait référence à la méthode de décarbonisation par acidification en solution (Appendice C).

APPENDICE B

PROCÉDURES DE LABORATOIRE DÉTAILLÉES

B1. Carbon and nitrogen analyses

Four different standards (acetanilide, cyclohexanone 2,4 dinitrophenylhydrazone, atropine, low organic content soil) and blanks were used to calibrate the equipment and verify the reproducibility ($R^2 \geq 0.999$ for nitrogen and $R^2 \geq 0.9999$ for carbon).

For fumigation, samples were weighted in silver cups and placed in a teflon tray, next to a beaker containing HCl 12N, both placed under a closed glass container for 24 hours. The silver cups were then wrapped into tin cups and placed into the elemental analyzer. For *acidification in solution*, HCl 1N was added to ~50 mg of each sample in test tubes and left to react for about 1 hour. Tubes were then centrifuged and the excess acid was removed. This protocol was repeated several times until neutral pH was attained. All samples were then transferred into aluminium foil covered beakers, frozen overnight and lyophilised for 4 days. The obtained organic carbon (OC) values using the *acidification in solution* method were

then corrected to take into account the loss of carbonates using the following equation: $C_{org} = 100 \times R_2 \times [1 - (R_2 - R_1) / (R_2 - 0.12)]$ where C_{org} is the weight percentage of organic carbon in the sample, R_2 is the weight percentage of carbon after acid treatment and R_1 is the weight percentage of total carbon.

Raw data was corrected with a calibration curve based on two reference material (-42.16‰; -17.14‰) normalized on the NBS19-LSVEC scale (Coplen et al., 2006). A third internal reference material was used to verify the precision of the calibration: -28.75‰. Results are presented in Appendix A, Table A4.

B2. Sedimentological analysis

Grain size analysis was performed using a Microtrac Bluelwave™ diffraction analyzer and softwares Microtrac FLEX™ 11.0.0.3 and GRADISTAT™. Statistical parameters were calculated using the method of moments in Microsoft Visual Basic programming language as well as linear interpolation by the Folk and Ward (1957) graphical method. The clay fraction corresponds to the size fraction inferior to 2 µm. The silt fraction lies between 2 and 63 µm, and the sand fraction is over 63 µm. For each sample, 2 ml of a solution, combining 0.25 g of wet sediment and 40 ml of milliQ water, was extracted using a pipette through a pierced lid at the center of a test tube. See results in Appendix A, Table A1.

Mineralogical composition was determined by x-ray diffraction using a Siemens Diffraktometer D5000TM with cobalt tube using the software DIFFRACTM to analyse and interpret the results.

B3. U-series isotopes analysis

Lead-210 activities were measured on an OrtecTM 476A alpha spectrometer along with the software MaestroTM. The bulk ground dried sediments of the 6 cores (every centimeter from the upper 12 cm) followed a systematic acid treatment protocol (Baskaran and Naidu, 1995). Uncertainties were estimated as $\pm 1\sigma$ standard deviation from counting statistics (2-4% of the value obtained).

Radium-226 activities were measured on an OrtecTM well detector of specific capacity of 10 cc. Radium-226 activity corresponds to the average activities of its daughters ^{214}Pb and ^{210}Bi assuming their secular radioactive equilibrium with radium 226. For this reason, the sample powder was weighted in plastic tubes and hermetically closed and left for 3 weeks to ensure that secular equilibrium was reached between radium and its daughters. Analysis was performed on bulk ground dried sediments from core PS87/030-3 (every centimetre from the upper 12 cm).

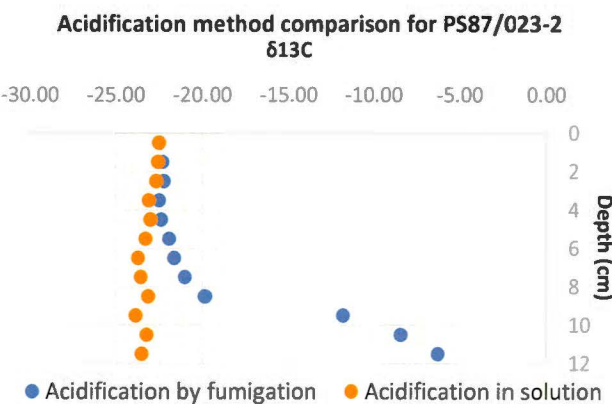
Thorium-230 measurements were made using a MC-ICPMS Nu-PlasmaTM II. Thorium-230 was measured on the ion counter while thorium-232 was measured on Faraday cups. The gain factor on the ion counter in ^{238}U - ^{235}U cups was monitored using uranium standard hu1 (^{235}U was measured on the first cycle on the ion

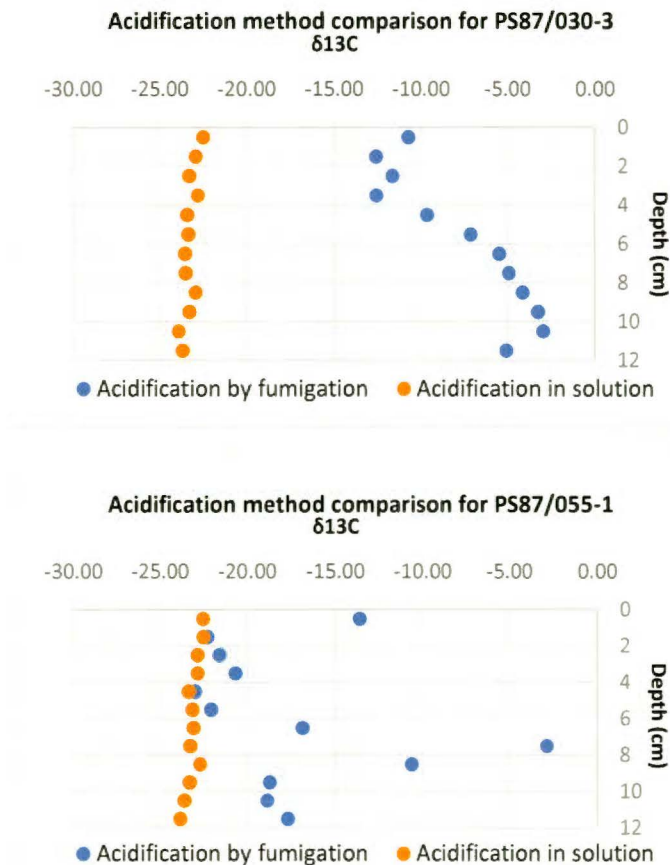
counter, then on the Faraday cup). The analytic protocol (Edwards et al, 1987) includes uranium and thorium separation and purification using anion exchange AG1x8 resin columns. Results are presented in Appendix A, Table A2.

APPENDICE C

COMPARAISON DES RÉSULTATS $\delta^{13}\text{C}$ DE DEUX MÉTHODES DE DÉCARBONISATION : ACIDIFICATION PAR FUMIGATION ET ACIDIFICATION EN SOLUTION

The following diagrams compare $\delta^{13}\text{C}$ measurements in organic carbon (OC) using two different decarbonation methods, one consisting in acidification by fumigation and the other consisting in acidification in solution. The comparative analysis, following the protocol of Hélie (2009) was done in three cores from the westernmost section of the Lomonosov Ridge (PS87/023-2; PS87/030-3; PS87/055-1).





The comparative analysis shows a wide range of $\delta^{13}\text{C}$ measurements between the two decarbonation methods for these three cores. As discussed in the article, measurements from acidification in solution in these cores are more consistent with $\delta^{13}\text{C}$ measurements for the easternmost cores, and with measurements obtained on Arctic sediments from previous studies. Given the higher concentration in more acid resistant carbonates (dolomite) in these cores (Appendix A, Table A3), acidification by fumigation on dolomite-rich sediments can lead to overestimations of $\delta^{13}\text{C}$.

APPENDICE D

DÉNOMBREMENT DE LA MICROFAUNE

Note : Les dénombrements présentés ici ont été réalisés par C. Brice (PS87/055-1) et P. Roberge (autres carottes).

carotte PS87/023-2	Profondeur (cm)	Dénombrement de la microfaune par type et par épaisseur de carotte										
		Foraminifères planctoniques (/g)	Foraminifères benthiques (/g)	Foraminifères agglutinants (/g)	Ostracodes (/g)	Épines d'échinodermes (/g)	Plaques d'échinodermes (/g)	Spicules (/g)	Bivalves (/g)	Diatomées (/g)	Radiolaires (/g)	Particules minérales (/g)
0.5	4796	48	0	7	0	0	7	0	0	0	0	239
1.5	1238	17	0	2	0	0	5	0	0	0	0	102
2.5	2039	76	0	5	0	0	4	1	0	0	0	287
3.5	2554	57	0	7	0	0	14	1	0	0	0	335
4.5	1812	39	0	4	0	0	8	0	0	0	0	233
5.5	1905	48	0	5	0	0	17	1	0	0	0	364
6.5	1605	22	0	11	0	0	9	2	0	0	0	509
7.5	335	12	0	9	0	0	3	2	0	0	0	461
8.5	268	19	0	11	0	0	8	2	0	0	0	732
9.5	1545	67	0	49	0	0	26	0	0	0	0	1692
10.5	3765	142	0	31	0	0	69	0	0	0	0	1242
11.5	3640	133	0	44	0	0	49	5	0	0	0	934
12.5	2140	87	0	19	0	0	27	2	0	0	0	1108
13.5	3294	86	0	24	0	0	8	0	0	0	0	773
14.5	3842	72	0	21	0	0	25	0	0	0	0	737
15.5	2580	54	0	14	0	0	2	0	0	0	0	634
16.5	2502	84	0	24	0	0	5	0	0	0	0	634
17.5	2192	69	0	13	0	0	6	0	0	0	0	414
18.5	2728	58	0	10	0	0	14	0	0	0	0	308

Carotte	Profondeur (cm)	Foraminifères planctoniques (/g)	Foraminifères benthiques (/g)	Foraminifères agglutinants (/g)	Ostracodes (/g)	Épines d'échinodermes (/g)	Plaques d'échinodermes (/g)	Spicules (/g)	Bivalves (/g)	Diatomées (/g)	Radiolaires (/g)	Particules minérales (/g)
PS87/055-1	0.5	5437	685	0	70	28	14	28	14	0	0	1593
	1.5	4785	305	0	136	11	11	45	0	0	0	1357
	2.5	5391	466	0	113	63	13	63	13	0	0	2419
	3.5	4646	604	0	46	23	0	12	0	0	0	1359
	4.5	2699	590	0	62	0	0	52	0	0	0	2730
	5.5	1836	551	0	99	8	8	31	0	0	0	2203
	6.5	1473	248	0	43	0	17	0	0	0	0	2201
	7.5	659	244	0	195	0	12	12	0	12	0	732
	8.5	429	112	0	31	0	0	7	0	3	0	507
	9.5	641	38	0	31	3	0	0	0	0	0	773
	10.5	722	42	0	28	4	4	0	0	0	0	912
	11.5	1456	100	0	82	6	0	0	0	0	0	1186
	12.5	1416	23	0	111	0	0	0	0	0	0	1236
	13.5	1106	59	0	118	0	0	0	0	0	0	1941
	14.5	849	33	0	66	0	0	0	0	0	0	1590
	15.5	575	17	0	43	0	2	0	0	0	0	860
	16.5	306	31	0	29	1	0	0	0	0	0	399
	17.5	560	203	0	63	8	0	3	0	3	0	552
	18.5	725	258	8	51	3	0	0	0	6	0	731
	19.5	1344	355	15	125	10	5	10	0	0	5	410
	20.5	4137	1101	26	335	9	0	17	0	0	34	920
	21.5	2003	259	16	141	16	0	8	8	0	8	1532
	22.5	1815	176	18	62	18	9	0	0	0	0	2431
	23.5	1985	129	0	37	0	0	0	0	0	0	2463
	24.5	1588	154	0	31	0	3	0	0	0	0	1402
	25.5	1632	258	13	32	13	6	6	0	0	0	1767

BIBLIOGRAPHIE

- Aagaard, K., & Carmack, E. C. (1989). The role of sea ice and other fresh water in the Arctic circulation. *Journal of Geophysical Research: Oceans*, 94(C10), 14485-14498.
<https://doi.org/10.1029/JC094iC10p14485>
- Assessment, A. C. I. (2004). Impacts of a Warming Arctic-Arctic Climate Impact Assessment. *Impacts of a Warming Arctic-Arctic Climate Impact Assessment, by Arctic Climate Impact Assessment*, pp. 144. ISBN 0521617782. Cambridge, UK: Cambridge University Press, December 2004., 144.
- Backman, J., Jakobsson, M., Løvlie, R., Polyak, L., & Febo, L. A. (2004). Is the central Arctic Ocean a sediment starved basin? *Quaternary Science Reviews*, 23(11-13), 1435-1454.
<https://doi.org/10.1016/j.quascirev.2003.12.005>
- Backman, J., Jakobsson, M., Frank, M., Sangiorgi, F., Brinkhuis, H., Stickley, C., ... & Gattacecca, J. (2008). Age model and core-seismic integration for the Cenozoic Arctic Coring Expedition sediments from the Lomonosov Ridge. *Paleoceanography*, 23(1).
<https://doi.org/10.1029/2007PA001476>
- Baskaran, M., & Naidu, A. S. (1995). 210 Pb-derived chronology and the fluxes of 210 Pb and 137 Cs isotopes into continental shelf sediments, East Chukchi Sea, Alaskan Arctic. *Geochimica et Cosmochimica Acta*, 59(21), 4435-4448.
- CliC/AMAP/IASC (2016), The Arctic Freshwater System in a Changing Climate. WCRP Climate and Cryosphere (CliC) Project, Arctic Monitoring and Assessment Programme (AMAP), International Arctic Science Committee (IASC).

Coplen, T. B., Brand, W. A., Gehre, M., Gröning, M., Meijer, H. A., Toman, B., & Verkouteren, R. M. (2006). New guidelines for $\delta^{13}\text{C}$ measurements. *Analytical Chemistry*, 78(7), 2439-2441. <https://doi.org/10.1021/ac052027c>

Coulthard, Roy D., et al. "New marine ΔR values for Arctic Canada." *Quaternary Geochronology* 5.4 (2010): 419-434.<https://doi.org/10.1016/j.quageo.2010.03.002>

Cranston, R. E. (1997). Organic carbon burial rates across the Arctic Ocean from the 1994 Arctic Ocean Section expedition. *Deep Sea Research Part II: Topical Studies in Oceanography*, 44(8), 1705-1723.[https://doi.org/10.1016/S0967-0645\(97\)00065-9](https://doi.org/10.1016/S0967-0645(97)00065-9)

Edwards, R.L., Chen, J.H., Wasserburg, G.J., 1987. ^{238}U ^{234}U ^{230}Th ^{232}Th systematic and the precise measurement of time over the past 500,000 years. *Earth and Planetary Science Letters* 81,175e192.

Frank, M., Backman, J., Jakobsson, M., Moran, K., O'Regan, M., King, Haley B. A, Kubik P. W., and Garbe-Schönberg, D. (2008). Beryllium isotopes in central Arctic Ocean sediments over the past 12.3 million years: Stratigraphic and paleoclimatic implications. *Paleoceanography*, 23(1). <https://doi.org/10.1029/2007PA001478>

Hélie, Jean-François (2009). Elemental and stable isotopic approaches for studying the organic and inorganic carbon components in natural samples. In *IOP Conference Series: Earth and Environmental Science* (Vol. 5, No. 1, p. 012005). IOP Publishing. <https://doi.org/10.1088/1755-1307/5/1/012005>

Huh, C. A., Pisias, N. G., Kelley, J. M., Maiti, T. C., & Grantz, A. (1997). Natural radionuclides and plutonium in sediments from the western Arctic Ocean: sedimentation rates and pathways of radionuclides. *Deep Sea Research Part II: Topical Studies in Oceanography*, 44(8), 1725-1743. [https://doi.org/10.1016/S0967-0645\(97\)00040-4](https://doi.org/10.1016/S0967-0645(97)00040-4)

- Jakobsson, M., Løvlie, R., Al-Hanbali, H., Arnold, E., Backman, J., & Mört, M. (2000). Manganese and color cycles in Arctic Ocean sediments constrain Pleistocene chronology. *Geology*, 28(1), 23-26. [https://doi.org/10.1130/0091-7613\(2000\)28<23:MACCIA>2.0.CO;2](https://doi.org/10.1130/0091-7613(2000)28<23:MACCIA>2.0.CO;2)
- Jakobsson, M., Backman, J., Murray, A., & Løvlie, R. (2003). Optically Stimulated Luminescence dating supports central Arctic Ocean cm-scale sedimentation rates. *Geochemistry, Geophysics, Geosystems*, 4(2). <https://doi.org/10.1029/2002GC000423>
- Jakobsson, M. et al. (2012). The international bathymetric chart of the Arctic Ocean (IBCAO) version 3.0. *Geophysical Research Letters*, 39(12). <https://doi.org/10.1029/2012GL052219>.
- Maccalini, J., Hillaire-Marcel, C., Carignan, J., & Reisberg, L. C. (2013). Geochemical signatures of sediments documenting Arctic sea-ice and water mass export through Fram Strait since the Last Glacial Maximum. *Quaternary Science Reviews*, 64, 136-151. <https://doi.org/10.1016/j.quascirev.2012.10.029>
- Not, C., Hillaire-Marcel, C., Ghaleb, B., Polyak, L., & Darby, D. (2008). ^{210}Pb - ^{226}Ra - ^{230}Th systematics in very low sedimentation rate sediments from the Mendeleev Ridge (Arctic Ocean). *Canadian Journal of Earth Sciences*, 45(11), 1207-1219. <https://doi.org/10.1139/E08-047>
- NSIDC: National Snow and Ice Data Center (2012a, septembre). Dans *Monthly archives*. "Arctic sea ice extent settles at record seasonal minimum." Récupéré de <http://nsidc.org/arcticseainews/2012/09/>
- NSIDC: National Snow and Ice Data Center (NSIDC) (2012b, novembre). Dans *Monthly archives*. "Arctic rapidly gaining winter ice." Récupéré de <http://nsidc.org/arcticseainews/2012/11/>

- O'Regan, M., King, J., Backman, J., Jakobsson, M., Pälike, H., Moran, K., Heil, C., Sakamoto, T., Cronin, T.M. & Jordan, R. W. (2008). Constraints on the Pleistocene chronology of sediments from the Lomonosov Ridge. *Paleoceanography*, 23(1). <https://doi.org/10.1029/2007PA001551>
- Polyak, L., Curry, W. B., Darby, D. A., Bischof, J., & Cronin, T. M. (2004). Contrasting glacial/interglacial regimes in the western Arctic Ocean as exemplified by a sedimentary record from the Mendeleev Ridge. *Palaeogeography, Palaeoclimatology, Palaeoecology*, 203(1-2), 73-93. [https://doi.org/10.1016/S0031-0182\(03\)00661-8](https://doi.org/10.1016/S0031-0182(03)00661-8)
- Screen, J. A., & Francis, J. A. (2016). Contribution of sea-ice loss to Arctic amplification is regulated by Pacific Ocean decadal variability. *Nature Climate Change*, 6(9), 856. <https://doi.org/10.1038/nclimate3011>
- Sellén, E., O'Regan, M., & Jakobsson, M. (2010). Spatial and temporal Arctic Ocean depositional regimes: a key to the evolution of ice drift and current patterns. *Quaternary Science Reviews*, 29(25-26), 3644-3664. <https://doi.org/10.1016/j.quascirev.2010.06.005>
- Stein, R. (2015). The expedition PS87 of the Research Vessel Polarstern to the Arctic Ocean in 2014. Alfred-Wegener-Institut, Helmholtz-Zentrum für Polar- und Meeresforschung. https://doi.org/10.2312/bzpm_0688_2015
- Yamamoto, M., Nam, S. I., Polyak, L., Kobayashi, D., Suzuki, K., Irino, T., & Shimada, K. (2017). Holocene dynamics in the Bering Strait inflow to the Arctic and the Beaufort Gyre circulation based on sedimentary records from the Chukchi Sea. *Climate of the Past*, 13(9), 1111. <https://doi.org/10.5194/cp-13-1111-2017>